9-1996

Global net carbon exchange and intra-annual atmospheric CO2 concentrations predicted by an Ecosystem Process Model and Three-Dimensional Atmospheric Transport Model

E. Raymond Hunt Jr.

Steve C. Piper

Ramakrishna R. Nemani

Charles D. Keeling

Ralf D. Otto

See next page for additional authors

Recommended Citation

Hunt Jr., E. R., S. C. Piper, R. Nemani, C. D. Keeling, R. D. Otto, and S. W. Running (1996), Global net carbon exchange and intra-annual atmospheric CO2 concentrations predicted by an ecosystem process model and three-dimensional atmospheric transport model, Global Biogeochem. Cycles, 10(3), 431–456, doi:10.1029/96GB01691.

GLOBAL BIOGEOCHEMICAL CYCLES, VOL. 10, NO. 3, PAGES 431–456, SEPTEMBER 1996

Global net carbon exchange and intra-annual atmospheric CO_2 concentrations predicted by an ecosystem process model and three-dimensional atmospheric transport model

E. Raymond Hunt Jr.,[1,2] Stephen C. Piper,[3] Ramakrishna Nemani,[1]
Charles D. Keeling,[3] Ralf D. Otto,[3,4] and Steven W. Running [1]

Abstract. A generalized terrestrial ecosystem process model, BIOME-BGC (for BIOME BioGeoChemical Cycles), was used to simulate the global fluxes of CO_2 resulting from photosynthesis, autotrophic respiration, and heterotrophic respiration. Daily meteorological data for the year 1987, gridded to 1° by 1°, were used to drive the model simulations. From the maximum value of the normalized difference vegetation index (NDVI) for 1987, the leaf area index for each grid cell was computed. Global NPP was estimated to be 52 Pg C, and global R_h was estimated to be 66 Pg C. Model predictions of the stable carbon isotopic ratio $^{13}C/^{12}C$ for C_3 and C_4 vegetation were in accord with values published in the literature, suggesting that our computations of total net photosynthesis, and thus NPP, are more reliable than R_h. For each grid cell, daily R_h was adjusted so that the annual total was equal to annual NPP, and the resulting net carbon fluxes were used as inputs to a three-dimensional atmospheric transport model (TM2) using wind data from 1987. We compared the spatial and seasonal patterns of NPP with a diagnostic NDVI model, where NPP was derived from biweekly NDVI data and *R*h was tuned to fit atmospheric CO_2 observations from three northern stations. To an encouraging degree, predictions from the BIOME-BGC model agreed in phase and amplitude with observed atmospheric CO_2 concentrations for 20° to 55°N, the zone in which the most complete data on ecosystem processes and meteorological input data are available. However, in the tropics and high northern latitudes, disagreements between simulated and measured CO_2 concentrations indicated areas where the model could be improved. We present here a methodology by which terrestrial ecosystem models can be tested globally, not by comparisons to homogeneous-plot data, but by seasonal and spatial consistency with a diagnostic NDVI model and atmospheric CO_2 observations.

Introduction

In order to better understand the role of terrestrial ecosystems in the global carbon cycle as affected by the interannual variability in global temperatures and precipitation, we are comparing anomalies of the atmospheric CO_2 record, hypothesized to be due to the interaction of ecosystem processes and climate [Keeling et al., 1995], with global predictions incorporating net primary production (NPP) and heterotrophic respiration (R_h), both of which are strongly controlled by climate. We are aided in characterizing these anomalies by having data on the $^{13}C/^{12}C$ isotopic ratio of atmospheric CO_2 in addition to concentration measurements. The concentration and isotopic data together permit a distinction to be made between oceanic and terrestrial contributions to these anomalies on shorter interannual time scales [Keeling et al., 1989b, 1995; Conway et al., 1994; Ciais et al., 1995; Francey et al., 1995], but do not explain the cause of the anomalies. Gaining this understanding requires an integrated modeling effort focusing on the seasonal cycle of atmospheric CO_2 concentrations and the interannual variability of the carbon cycle. Input data for prediction of the ecosystem processes must be from as close to the actual data as possible, not based on potential vegetation or long-term climatic averages, for understanding of the atmospheric CO_2 anomalies.

There are many ecosystem process models which help to explain terrestrial net primary production and heterotrophic respiration: the Terrestrial Ecosystem Model (TEM) by Melillo et al. [1993], the Carnegie Ames Stanford Approach (CASA) by Potter et al. [1993], the Frankfurt Biosphere Model (FBM) by Lüdeke et al. [1994], the Carbon Assimilation in the Biosphere model (CARAIB) by Warnant et al. [1994], the Century model by Parton et al. [1987, 1993], and the Land Surface Model (LSM) by Bonan [1995] to name just a few. Each model, however, has been designed for a specific purpose and makes assumptions to simplify ecosystem processes which do not compromise that particular purpose. Some of these models thus do not simulate a complete hydrologic budget and hence can neither predict short-term decreases in NPP due to drought nor the effects of moisture storage in the soil. Others use mean monthly climatological data and potential vegetation, so the

[1] School of Forestry, University of Montana, Missoula.
[2] Now at Department of Botany, University of Wyoming, Laramie.
[3] Scripps Institution of Oceanography, La Jolla, California.
[4] Now at Institut für Physikalische and Theoretische Chemie, J. W. Goethe Universität, Frankfurt am Main, Germany.

Paper number 96GB01691.
0886-6236/96/96GB-01691$12.00

effects on vegetation of interannual variability in precipitation and temperature cannot be realistically simulated. Thus most of the existing ecosystem models are not optimal for direct comparisons with atmospheric CO_2 anomaliesbecause of the interannual variability of climate.

Patterns of vegetation activity are described globally by the normalized difference vegetation index (NDVI) from the Advanced Very High Resolution Radiometer, AVHRR [Goward et al., 1985; Fung et al., 1987]. There are several models which estimate NPP from NDVI, which are based on the premise that NDVI can be used to estimate the fraction of photosynthetically active radiation (PAR) absorbed by vegetation [Kumar and Monteith, 1981]. The primary advantage of diagnostic NDVI models is their simplicity based on remotely sensed data, with a trade-off that these models are not usually mechanistic. Sellers et al. [1992] combined leaf level photosynthesis and radiative transport models to demostrate that vegetation indices measure the fraction of absorbed PAR by vegetation, showing simple NDVI models are useful in estimating NPP. The estimated CO_2 exchanges from a refined diagnostic NDVI model were then also used as inputs to an atmospheric CO_2 tracer model [Heimann and Keeling, 1989; Heimann, 1995], to predict the atmospheric CO_2 concentrations at various locations throughout the world.

We report here on progress in characterizing net carbon exchange globally by an ecosystem process model, BIOME-BGC (for BIOME-BioGeoChemical cyles), designed to simulate interannual variability in net primary production and heterotrophic respiration on a global scale using daily weather data and portraying, as close as possible, the actual conditions of vegetation and soils [Hunt and Running, 1992a; Running and Hunt, 1993]. BIOME-BGC is sensitive to leaf area index (LAI), which we estimate using the maximum value of NDVI for a specific year. The model uses a daily time step to predict the hydrologic and carbon fluxes by means of basic physiological principles, and it calculates the uptake of the stable carbon isotope ^{13}C as a means to relate observations of ^{13}C in atmospheric CO_2. The objectives of this paper are: (1) to present our logic and preliminary computations of the global carbon fluxes for a single year, 1987, and (2) to compare seasonal predictions of atmospheric CO_2 concentrations from both the BIOME-BGC model and a diagnostic NDVI model with direct observations from monitoring stations. These comparisons provide a methodology for testing terrestrial ecosystem process models at global scales rather than testing at local scales with homogeneous plot data.

Implementation of BIOME-BGC for Global Simulations

BIOME-BGC simulates the carbon, hydrologic, and nitrogen cycles for a generalized ecosystem [Hunt and Running, 1992a; Running and Hunt, 1993]. This model was developed from a coniferous forest ecosystem model, FOREST-BGC [Running and Coughlan, 1988; Running and Gower, 1991], and has undergone extensive validation of the simulated water and carbon budgets in different North American ecosystems [Nemani and Running, 1989a; Korol et al., 1991; Hunt et al., 1991b; Running, 1994; Rollins, 1995].

The model has two time steps (Figure 1): a daily time step in which all-sided leaf area index (LAI) is used for the simulation of photosynthesis, autotrophic and heterotrophic respiration, and the hydrologic budget (Figure 1), and an annual time step for allocation of carbon and nitrogen, litterfall and turnover, and net nitrogen mineralization. The inputs and outputs of this model are presented in Table 1. The symbols and units are presented in the notation list. The daily timestep of BIOME-BGC is very important and will be described in detail in Appendix A. In this preliminary study, the annual time step is not important for the purposes of

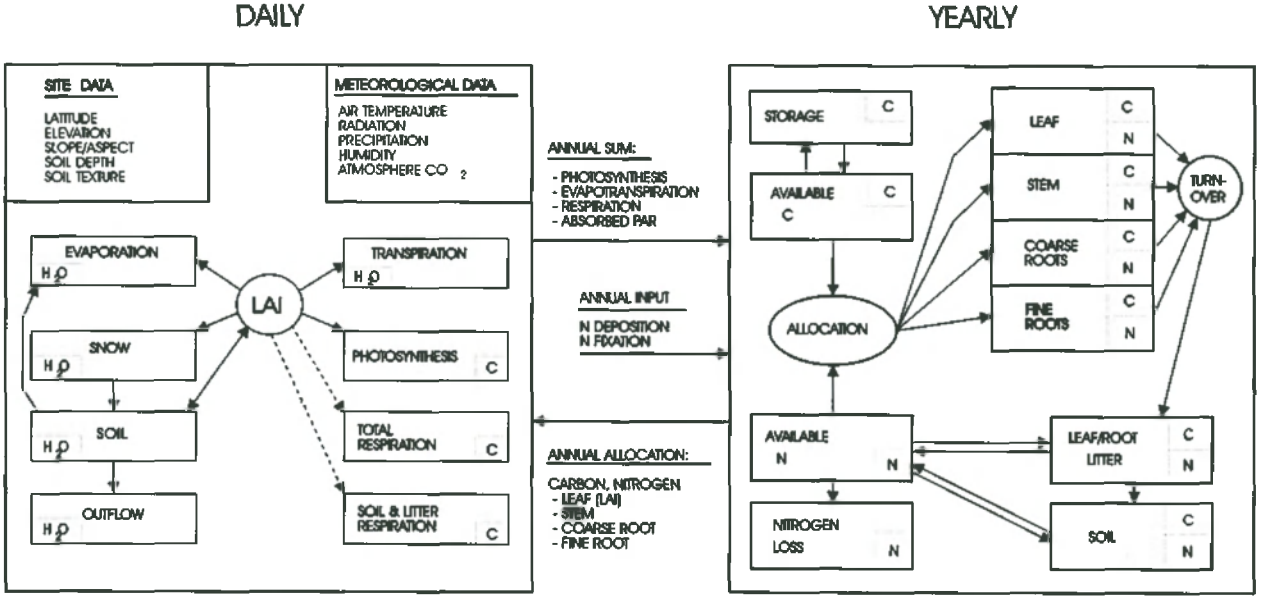

Figure 1. BIOME-BGC flow chart. Leaf area index (LAI) directly affects canopy processes (shown by solid arrows) and indirectly affects soil processes by affecting soil temperature for the daily time step. The yearly time step is for the allocation of carbon and nitrogen among leaves, stems, coarse and fine roots, litter, and soil. As we are simulating net primary production and heterotrophic respiration for 1987 only, the yearly time step has no effect on the predictions. This ecosystem model is based on leaf area index data derived from remote sensing.

Table 1. Data Inputs and Outputs to BIOME-BGC

	Unit of Measure
Required inputs for each grid cell	
Latitude	degrees
Elevation	m
Vegetation cover type	
Leaf area index (LAI)	$m^2\ m^{-2}$
Soil texture class	
Soil depth (corrected for coarse fragments)	m
Soil carbon content	kg C ha^{-1}
Initial soil water content	$m^3\ ha^{-1}$
Initial snowpack	$m^3\ ha^{-1}$
Initial soil temperature at 10 cm depth	°C
Required daily inputs	
Air temperature, maximum	°C
Air temperature, minimum	°C
Precipitation (water equivalent)	mm d^{-1}
Calculated or optional inputs	
Daylength	s
Daily solar radiation	kJ $m^{-2}\ d^{-1}$
Photosynthetically active radiation (noon)	μmol $m^{-2}\ s^{-1}$
Average daytime relative humidity	dimensionless
Soil temperature at 10 cm depth	°C
Atmospheric CO_2	ppm
Daily outputs	
Water fluxes: transpiration, evaporation, outflow	$m^3\ ha^{-1}\ d^{-1}$
Soil water content	$m^3\ ha^{-1}$
Predawn leaf/soil water potential	MPa
Gross photosynthesis	kg C $ha^{-1}\ d^{-1}$
Autotrophic respiration	kg C $ha^{-1}\ d^{-1}$
Heterotrophic respiration	kg C $ha^{-1}\ d^{-1}$
Net ecosystem exchange	kg C $ha^{-1}\ d^{-1}$
Net ecosystem ^{13}C flux	kg ^{13}C $ha^{-1}\ d^{-1}$
Absorbed PAR	MJ $m^{-2}\ d^{-1}$
Annual outputs	
Net primary production	kg C $ha^{-1}\ year^{-1}$
Heterotrophic respiration	kg C $ha^{-1}\ year^{-1}$
Net ecosystem exchange	g C $ha^{-1}\ year^{-1}$
PAR conversion efficiency	g dry weight MJ^{-1}
Vegetation $\delta^{13}C$	dimensionless

simulating the global carbon fluxes for 1987 and will be described only briefly in Appendix A. However, as R_h is extremely dependent on litter from the previous year's NPP, the annual time step is essential for understanding the role of terrestrial ecosystems in causing the year-to-year differences in atmospheric CO_2 anomalies.

Definition of Land Cover Type

To define land cover types, we used four key features of vegetation that strongly control ecosystem fluxes of carbon, water and nitrogen [Running and Hunt, 1993; Running et al., 1995]. The first is photosynthetic pathway, either C_3 photosynthesis or C_4 photosynthesis. The second is the presence of permanent biomass aboveground (wood) affecting autotrophic respiration and aerodynamic conductances. The third is leaf longevity (evergreen or deciduous) affecting photosynthetic rate, autotrophic respiration, and heterotrophic respiration via the nitrogen and lignin concentrations of the foliage. The fourth feature is leaf morphology (grass, needleleaf or broadleaf) which affects radiation absorption and remotely sensed vegetation indices. Not all combinations of these four features occur as a land cover type; thus we defined the following six of seven classes: (1) C_3 grasslands (including C_3 agricultural areas and tundra), (2) C_4 grasslands (including C_4 agricultural areas and savannas), (3) evergreen broadleaf forests (mostly tropical evergreen rainforests), (4) deciduous broadleaf forests (most potential regions are now mostly agriculture), (5) evergreen needleleaf forests (coniferous forests), and (6) deciduous needleleaf forests (*Larix* forests). A seventh category, shrub lands, is also defined for areas which could be classified either as evergreen or deciduous "broadleaf forests," except that the physiological differences between shrub lands and other broadleaf forests are so large that a separate category is required.

The global potential vegetation map of Matthews [1983] was the starting point for generation of the land cover types for these

Table 2. BIOME-BGC Biological Parameters for Different Land Cover Types

Parameter[a]	C_3G	C_4G	EN	DN	EB	DB	Sh
Ratio of total LAI to one-sided LAI	2.0	2.0	2.4	2.4	2.0	2.0	2.0
Specific leaf area (m^2 kg C^{-1})	40.	40.	20.	50.	35.	65.	25.
Aerodynamic conductance (mm s^{-1})	0.01	0.01	1.0	1.0	1.0	1.0	0.1
Maximum stomatal conductance (mm s^{-1})	5.0	2.0	2.2	4.5	4.0	4.5	3.5
Water potential at stomatal closure (Mpa)	-2.5	-4.0	-1.6	-1.6	-1.6	-1.6	-5.5
Vapor pressure difference at stomatal closure (kPa)	3.5	4.5	2.5	2.5	2.5	2.5	3.5
Maximum photosynthetic rate (μmol $m^{-2}\ s^{-1}$)	6.0	7.5	3.5	5.0	4.0	5.0	3.5
Optimum temperature (°C)	20.	30.	20.	20.	20.	20.	20.
Leaf maintenance respiration (g $kg^{-1}\ d^{-1}$)	5.0	5.0	1.2	3.0	1.5	4.0	1.2
Leaf lignin concentration (%)	17.	17.	27.	17.	27.	17.	27.
Leaf turnover (%)	100	100	33.	100	33.	33.	100
Maximum height (m)	0.5	0.5	30.	30.	30.	30.	5.0

C_3G, C_3 grassland; C_4G, C_4 grassland; EN, evergreen needleleaf; DN, deciduous needleleaf; EB, evergreen broadleaf; DB, deciduous broadleaf; Sh, shrubland. Annual crops are assumed to have the same biological parameters as C_3 grasses or C_4 grasses.

[a] Parameters are based on total (all-sided) LAI.

Table 3. Classification of Matthews Vegetation Classes in Land Cover Types

Vegetation Class and Description	Type[a]	Longevity[b]
1 Tropical evergreen, mangrove forest	B	E
2 Tropical/subtropical evergreen seasonal forest	B	E
3 Subtropical evergreen rainforest	B	E
4 Temperate/subpolar evergreen rainforest	B	E
5 Temperate evergreen seasonal broadleaved forest, summer rain	B	E
6 Evergreen broadleaved sclerophyllous forest, winter rain	S	E
7 Tropical/subtropical evergreen needleleaved forest	N	E
8 Temperate/subpolar evergreen needleleaved forest	N	E
9 Tropical/subtropical drought-deciduous forest	B	D
10 Cold-deciduous forest with evergreens	B	D
11 Cold-deciduous forest without evergreens	B	D
12 Xeromorphic forest/ woodland	S	D
13 Evergreen broadleaved sclerophyllous woodland	S	E
14 Evergreen needleleaved woodland	N	E
15 Tropical/subtropical drought-deciduous woodland	B	D
16 Cold-deciduous woodland	N	D
17 Evergreen broadleaved shrubland/ thicket, evergreen dwarf-shrubland	S	E
18 Evergreen needleleaved/microphyllous shrubland/thicket	S	E
19 Drought-deciduous shrubland/thicket	S	D
20 Cold-deciduous supalpine/subpolar shrubland, dwarf shrubland	S	D
21 Xeromorphic shrubland/dwarf shrubland	S	D
22 Arctic/alpine tundra, mossy bog	G	D
23 Tall/medium/short grassland with 10-40% woody cover	G	D
24 Tall/medium/short grassland with < 10% woody cover	G	D
25 Tall/medium/short grassland with shrub cover	G	D
26 Tall grassland, no woody cover	G	D
27 Medium grassland, no woody cover	G	D
28 Meadow, short grassland, no woody cover	G	D
29 Desert	na	na
30 Ice	na	na
31 Cultivation	G	D

Abbreviation na indicates not applicable.

[a] Types: N, needleleaf; B, broadleaved; S, shrubland, G, grass.

[b] Longevities: D, deciduous; E, evergreen.

simulations at a resolution of 1° latitude by 1° longitude. This data set was obtained from the Global Ecosystems Database (Version 1.0 on CD-ROM) from Kineman and Ohrenschall [1992]. We reclassified the 31 vegetation classes of the Matthews' data set into four leaf morphology types and two leaf longevity classes (Tables 2 and 3). All grid cells with at least 50% cultivation intensity in the Matthews' [1983] data set were assigned to grasslands in order to approximate current actual vegetation. The separation of grasslands into C_3 and C_4 was estimated from the distributions of the minimum and maximum values of mean monthly temperature obtained from the International Institute of Applied Systems Analysis Mean Monthly Temperature data set [Leemans and Cramer, 1991; Kineman and Ohrenschall, 1992]. We assumed C_4 grasslands occupy areas where both the minimum value was over a threshold of -1°C and the maximum value was over a threshold of 22°C [Teeri, 1977]. Finally, using the classification of Loveland et al. [1991], we changed the C_3 grasslands for longitudes from 83°W to 97°W and latitudes from 40°N to 44°N to C_4 grasslands to account for the large C "cornbelt" in the United States of America. Our preliminary map of actual land cover is shown in Plate 1. Ongoing studies using AVHRR data will improve the classification of land cover types [DeFries and Townsend, 1994; Nemani and Running, 1995, 1996] for our continuing work.

Almost half of the land area of the globe was either C_3 or C_4 grasslands (Table 4), consistent with Houghton [1994], because of our assignment of agricultural areas as grasses. Deciduous needleleaf forests were the least abundant, principally occurring in Russia (Plate 1). The other four land cover types occurred over approximately equal areas globally (Plate 1 and Table 4).

Leaf Area Index (LAI) and State Variable Initializations

We examined the monthly experimental global normalized difference vegetation index (NDVI) data [Gallo, 1992], to obtain the maximum NDVI for each 1° latitude by 1° longitude terrestrial grid cell for 1987. To minimize the impact of cloud contamination and atmospheric influences, we then compared this 1987 maximum value of NDVI with the mean of the maximum values for years from 1985 to 1990; whenever the 1987 maximum was 0.10 less than the mean maximum NDVI for the 6 years of record, we substituted the mean NDVI for the 1987 value. This occurred for only 76 grid cells scattered worldwide, primarily in coastal areas.

To account for the differences in structural and optical properties of canopies among different vegetation types, we used separate NDVI-one-sided LAI relations for grasslands, needleleaf forests, and broadleaf forests. The equation for grasslands and shrub lands is

$$LAI = 1.71\ NDVI + 0.48 \quad (1)$$

[Nemani and Running, 1995], for needleleaf forests is

$$LAI = (3.23\ NDVI)^{2.6} \quad (2)$$

[Spanner et al., 1990; Nemani and Running, 1989a], and for broadleaf forests is

$$LAI = (3.85\ NDVI)^{2} \quad (3)$$

[Pierce et al., 1993]. These empirical relations based on field studies were found to agree with theoretically derived forms of NDVI-LAI relations [Asrar et al., 1992; Sellers et al., 1994]. We acknowledge that these simple empirical relations do not account for problems such as variations in background, atmospheric influences, and viewing geometry; however, using only the annual maximum NDVI value for each grid cell reduces the impacts of these problems [Nemani and Running, 1996]. All-sided LAI is

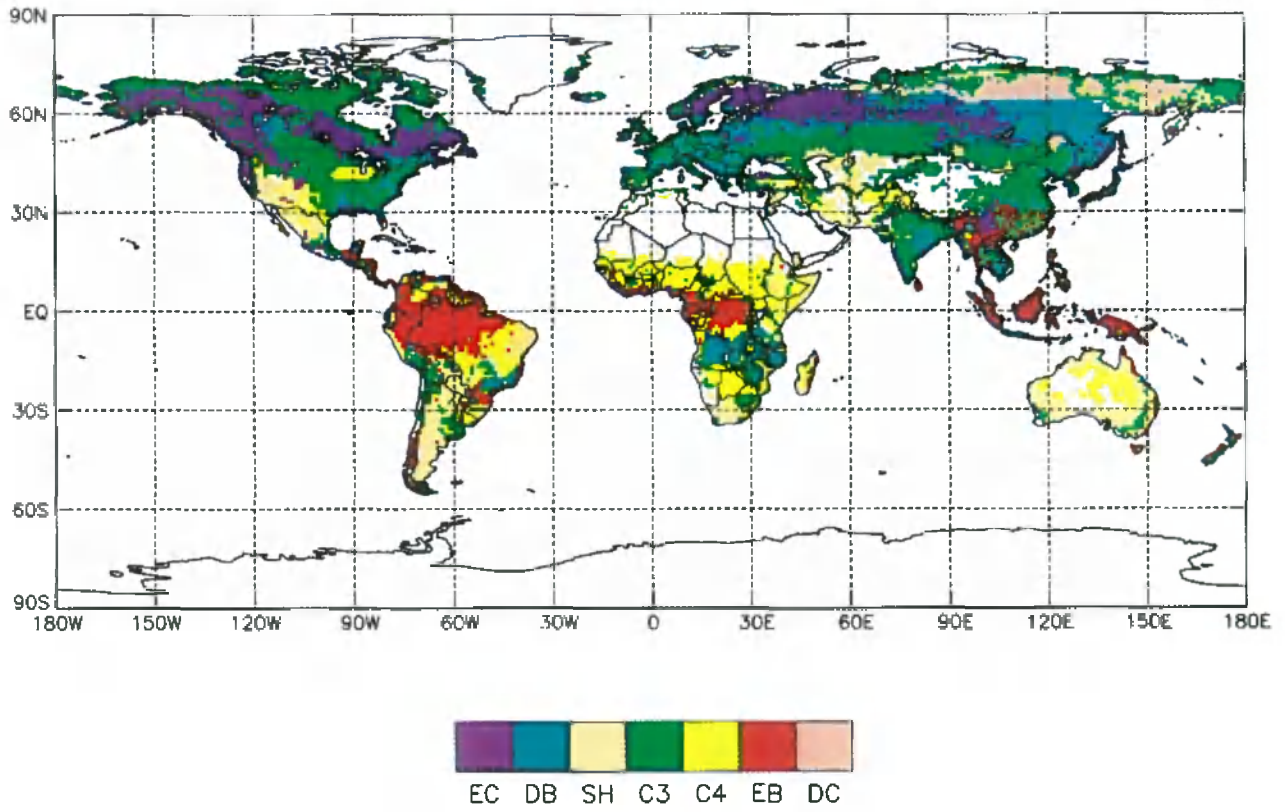

Plate 1. Land cover types (1° latitude by 1° longitude) modified from Matthews [1983] potential vegetation and percent agriculture. White areas on land in this and following map figures represent regions of desert or ice, which were not considered further.

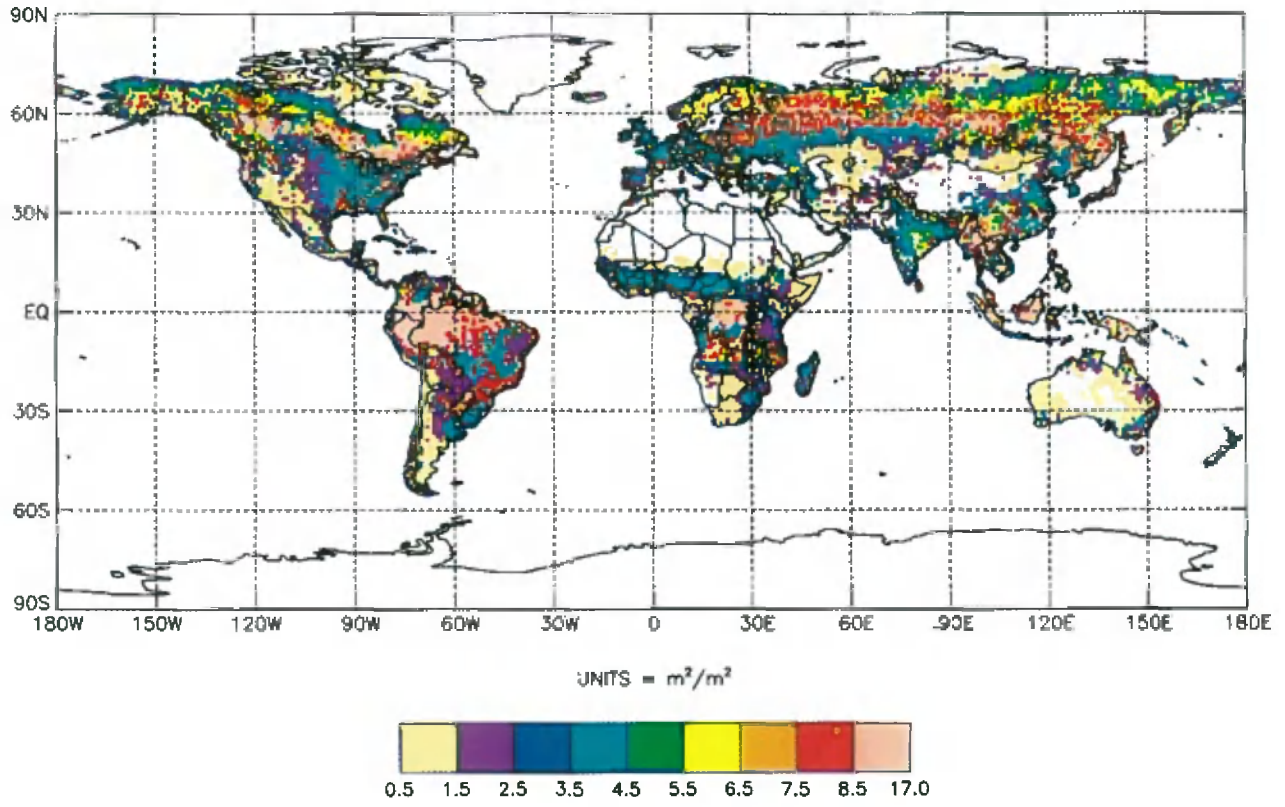

Plate 2. Leaf area index for 1987 (1° latitude by 1° longitude) determined using annual maximum values of normalized difference vegetation index from Gallo [1992].

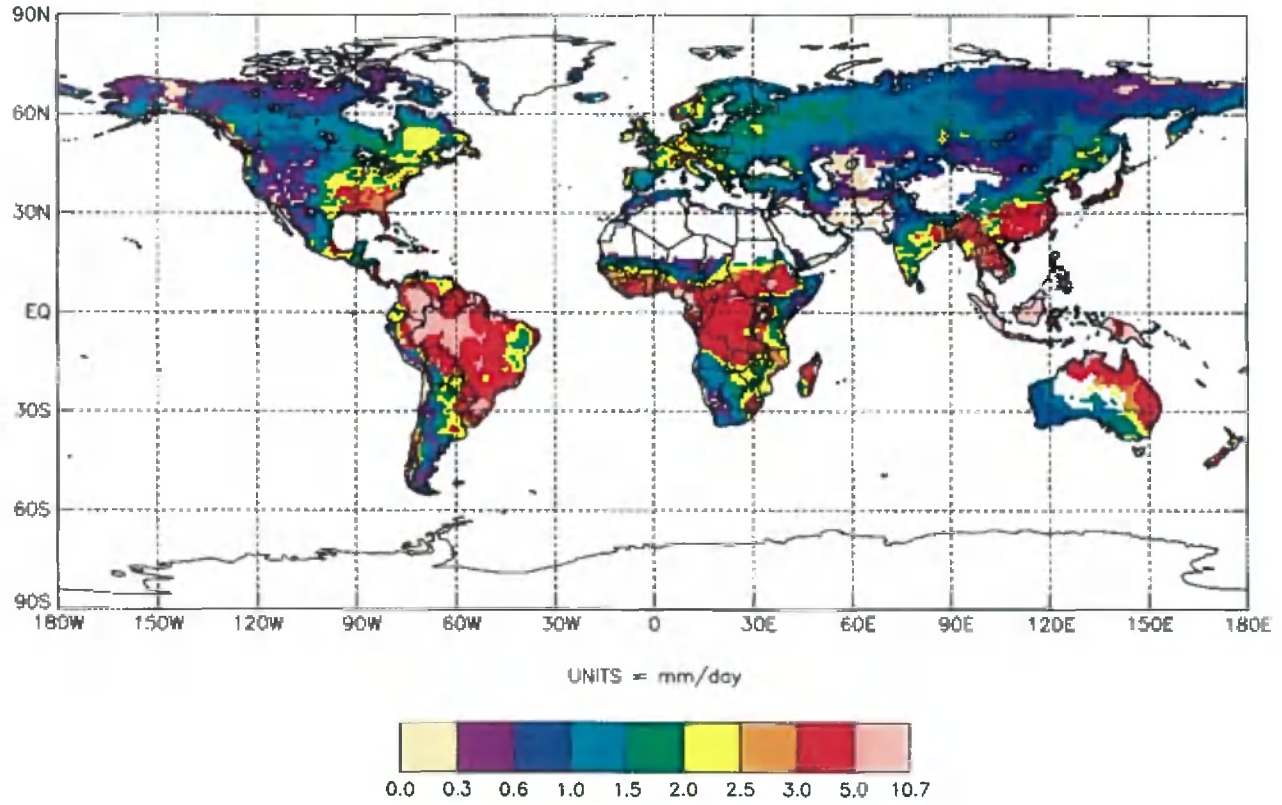

Plate 3. Annual mean of daily precipitation for 1987 (1° latitude by 1° longitude) using data from Piper [1995]. Total annual precipitation for each grid cell is determined by multiplying the mean by 365.

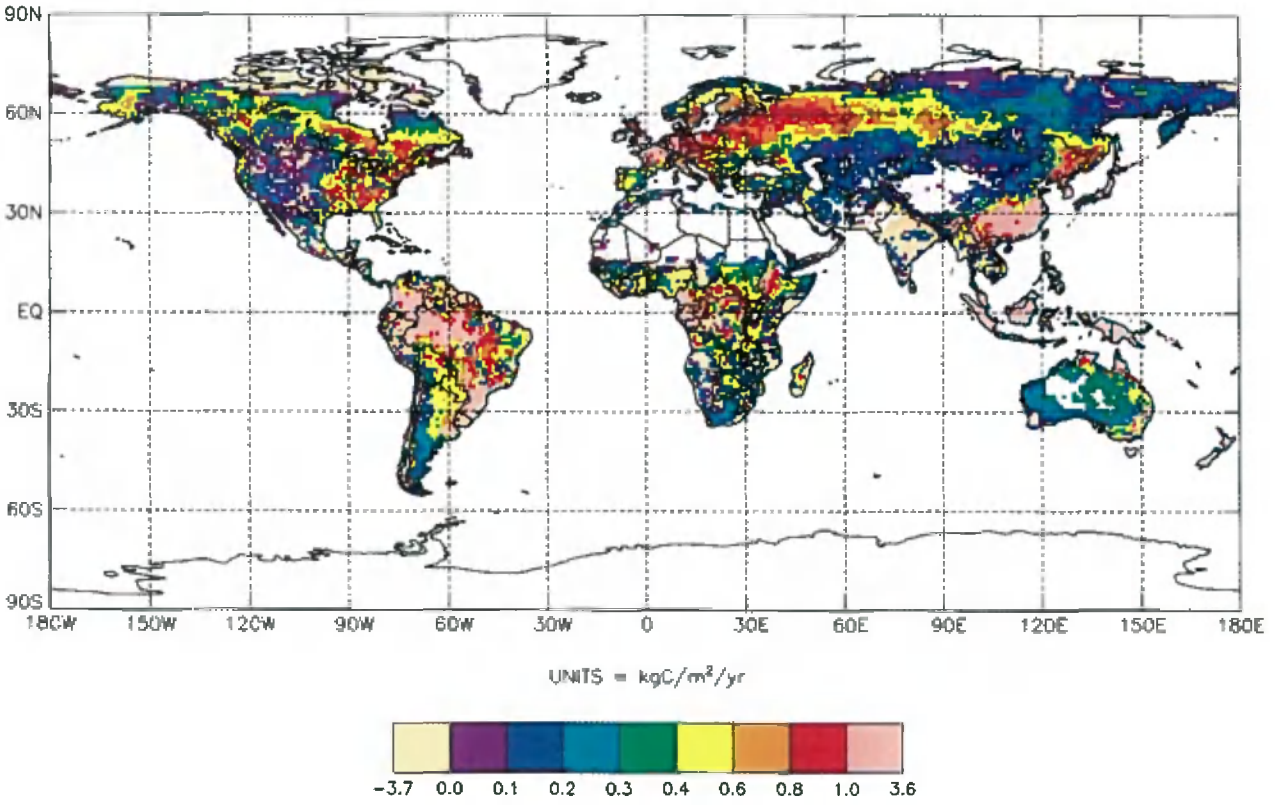

Plate 4. Simulated annual net primary production for 1987 (1° latitude by 1° longitude). The global total of net primary production is 52.0 Pg C.

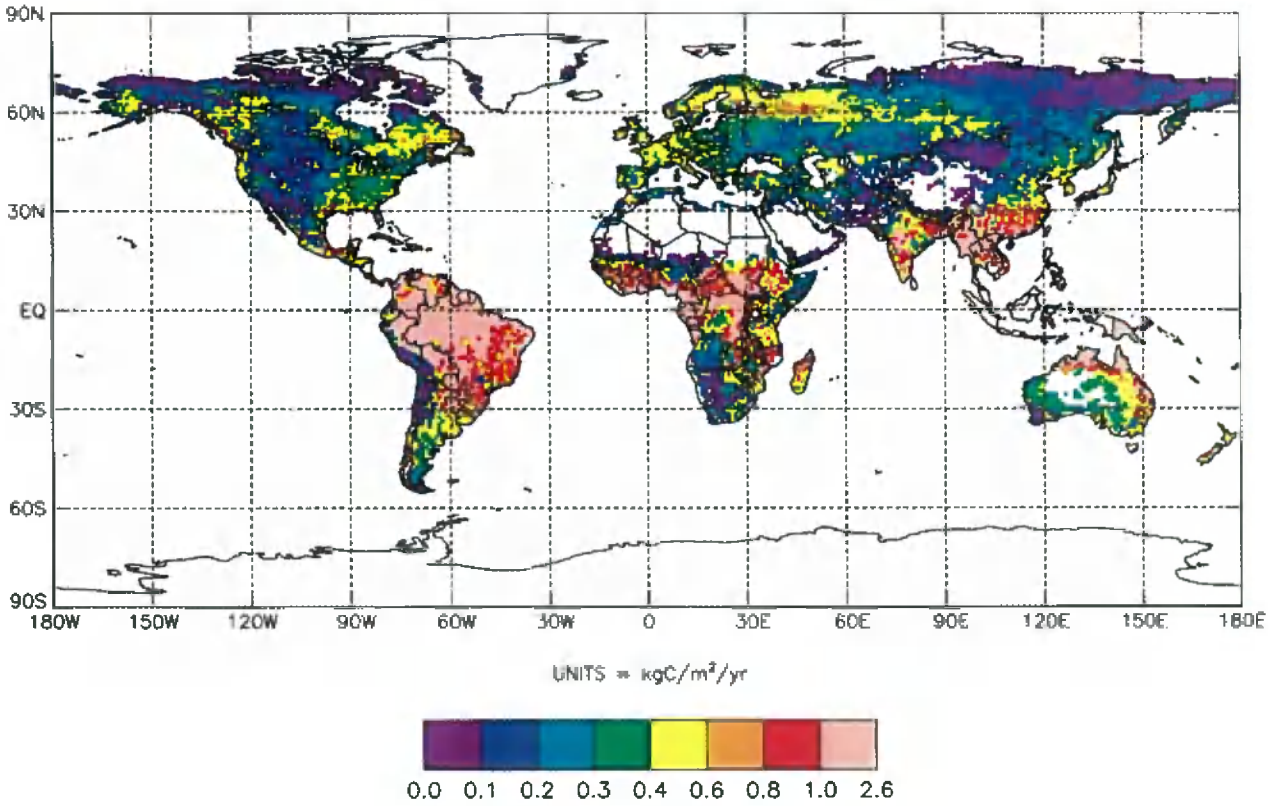

Plate 5. Simulated annual heterotrophic respiration for 1987 (1° latitude by 1° longitude). The global total of heterotrophic respiration is 65.6 Pg C, before adjustment.

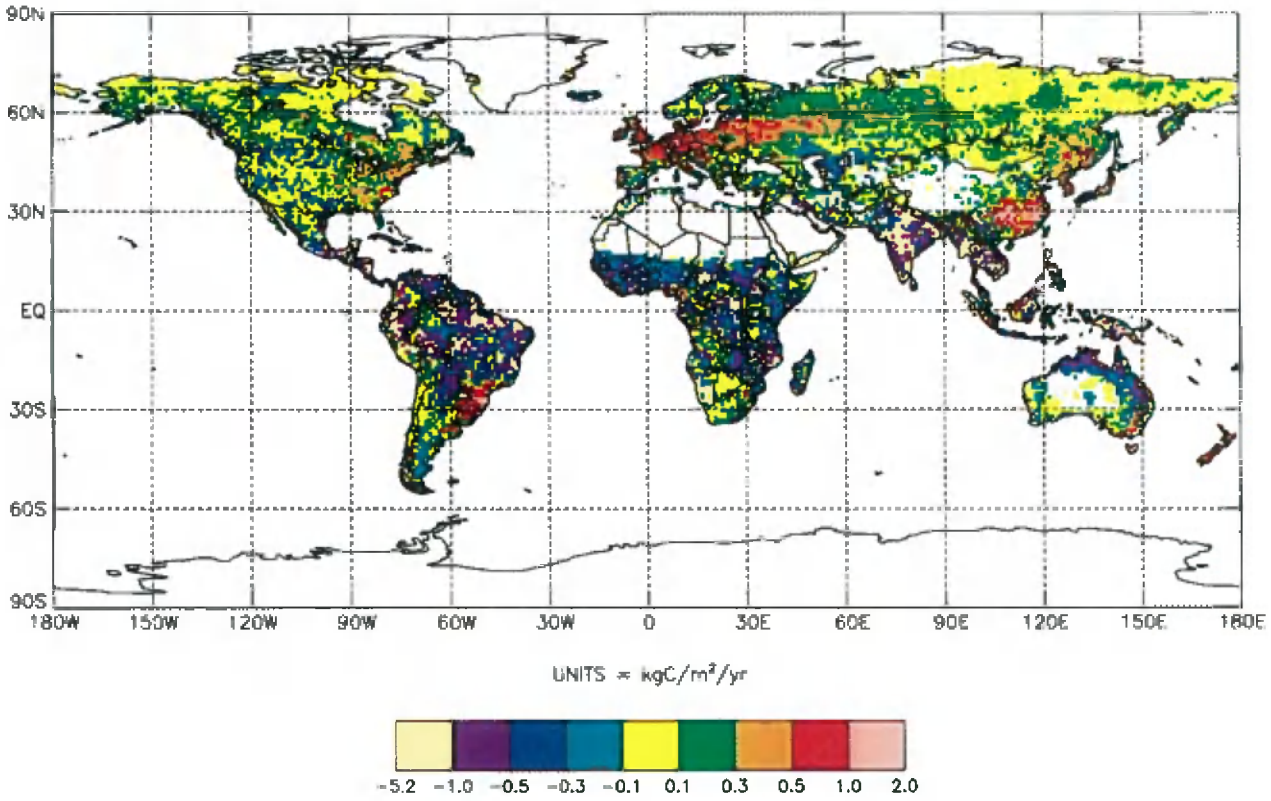

Plate 6. Simulated annual net ecosystem exchange (NEE) for 1987 (1° latitude by 1° longitude), which is the difference between annual NPP and R_h. The global total of NEE was -13.6 Pg C.

Table 4. Biome Totals of Area and Carbon, and Mean Leaf Area Indices

Land cover type	Area[a] 10^6 km^2	Leaf C, Pg	Mean LAI	Stem C, Pg	Soil C, Pg
C3 grassland	34	2.5	2.9	0.0	351
C4 grassland	20	1.3	2.6	0.0	159
Evergreen needleleaf	12	4.3	7.2	102	190
Deciduous needleleaf	2.5	0.25	5.0	10.1	32
Evergreen broadleaf	17	4.3	8.9	224	169
Deciduous broadleaf	14	1.5	7.0	111	167
Shrub land	18	1.7	2.4	10.9	130
Totals	117	15.9		458	1198

[a] Not including areas classified initially as barren desert or ice.

calculated from a ratio specified for each land cover type (Table 2). Our map of all-sided maximum LAI is shown in Plate 2. Table 4 shows the global averages of all-sided LAI for each land cover type.

Soil Carbon and Water Holding Capacity

Following Post et al. [1982] and Potter et al. [1993], we assumed that soil carbon is related to potential land cover type. We obtained the Leemans [1990] Holdridge Life Zone classification from Kineman and Ohrenschall [1992] and generated a map of soil carbon mass M_{soil}. We then assumed a soil carbon to nitrogen ratio of 12 [Parton et al., 1987] to estimate the amount of soil nitrogen.

We used the Zobler soil texture database [Zobler, 1986] from Kineman and Ohrenschall [1992] to estimate the soil water content at field capacity Θ_{max}. We assigned textures (percents of sand, silt, and clay) to each Zobler class. Then, Θ_{max} was calculated for each grid cell by inverting the equations of Saxton et al. [1986], assuming that Ψ_{soil} at field capacity equals -0.025 MPa.

Soil depth was set at 1 m for all grid cells, not including coarse fragments, which add to depth but not to the storage of soil moisture. Whereas coarse roots of most vegetation can easily go to depths of 2 m or more [Webb et al., 1993, Table 4], most of the fine roots which absorb mineralized nutrients and water occur at much shallower depths. Deep coarse roots have significantly smaller conductances to lateral and axial water flow and require a large water potential gradient between leaf and soil to move significant amounts of water [Hunt et al., 1991a]. Thus we assume deep roots are probably required to survive drought but should not be expected to transport water from deep in the soil to sustain maximum rates of transpiration. However, recent work by Nepstad et al. [1994] casts doubt on this assumption for some tropical forest ecosystems.

Climatic Inputs

We used the global gridded temperature and precipitation data set for 1987 from Piper [1995] and Piper and Stewart [1996]. These data were daily maximum air temperature, daily minimum air temperature, and water-equivalent precipitation gridded to 1° latitude by 1° longitude for the land surface. Station summary-of-the-day records produced by the U.S. Climate Prediction Center (CPC) were used as the basis for gridding the data. These daily station records were summarized from the archive of synoptic reports received over the Global Telecommunications System at the U.S. National Centers for Environmental Prediction primarily from the World Meteorological Organization global synoptic surface network of stations.

The station data, which had undergone quality tests at CPC to correct for transmission and observational errors, were subjected to an additional series of quality checks in which errors and omissions in station locations, duplicate records and redundant stations, and extreme outliers were identified and either deleted or corrected [Piper, 1995]. No attempt was made to correct for the systematic underestimation of precipitation by rain gauges [e.g., Legates, 1987] nor for station relocations, heat island effects, or instrument changes. The final corrected data set contains temperature data for 6610 stations and precipitation data for 6172 stations.

The daily station data were then interpolated to a 1° by 1° degree grid by using the nearest-neighbor weighting scheme of Shepard [1968], as modified for spherical coordinates by Willmott et al. [1985]. The mean elevation of the grid cells was calculated as the area-weighted average of the 5 arc min elevations provided in the global topography data set ETOPO5 [National Geophysical Data Center, 1988]. To reduce problems associated with

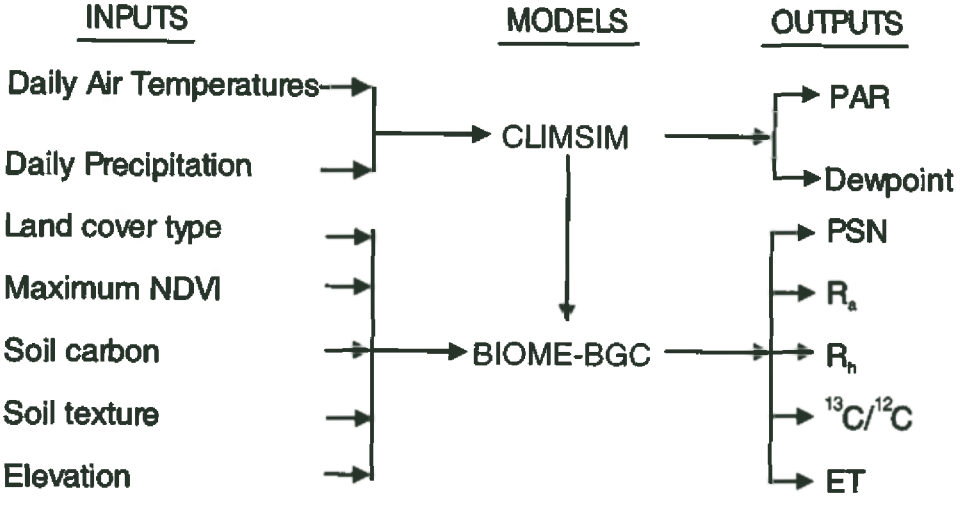

Figure 2. Global Ecosystem Simulation System (GESSys) flow chart of data inputs, models, and simulated outputs.

Table 5. Locations of Atmospheric CO_2 Sampling Stations

Station	Latitude	Longitude
Point Barrow, Alaska (PTB)	71°N	157°W
Cold Bay, Alaska (CBA)	55°N	163°W
La Jolla, California (LJO)	33°N	117°W
Mauna Loa, Hawaii (MLO)	20°N	156°W
Cape Kumukahi, Hawaii (KUM)	20°N	155°W
Christmas Island (CHR)	2°N	159°W
Baring Head, New Zealand (NZD)	41°S	175°E
South pole (SPO)	90°S	0°W

topographic variations, temperatures were adjusted to sea level, assuming a uniform environmental lapse rate of -6.5°C per 1000 m altitude. Using the same lapse rate, temperatures were then re-adjusted to the mean elevation of each grid cell after interpolation. Precipitation data were interpolated without adjustment for elevation.

The year, 1987, was part of an El Niño episode that extended from 1986 into 1988; such episodes are associated with climate anomalies worldwide [Ropelewski and Halpert, 1987]. Accordingly, much of North America exhibited warmer than normal temperatures in winter and spring; the extreme was 6°C above normal for December 1986 through April 1987 in central Canada [World Climate Data Programme, 1987]. The western United States, southwestern Canada and the Great Lakes region were abnormally dry through spring. East central Brazil was unusually dry during January and February, and northern Argentina and southern Brazil were dry in September and October. Southeastern Europe experienced abnormally warm and dry conditions in June, July, and September.

The monsoon in India was weak; parts of India and Pakistan had less than half of the expected rainfall for the usual monsoon period. Unusually heavy rains flooded parts of China, Taiwan and Korea in late July and August. In the western African Sahel region, precipitation was abnormally low. Eastern central Africa received less than half of the normal precipitation from October through December. Each of these anomalies was identified, qualitatively, in the data set of Piper [1995] by comparisons with the Leemans and Cramer [1991] climatology at a 1° by 1° grid resolution. The abnormally dry conditions that prevailed in Australia during 1987 [World Climate Data Programme, 1988] are not well represented in this data set [Piper, 1995] because of sparse station data. The mean daily precipitation for each grid cell (Plate 3) shows a similar pattern to LAI, where the mean daily amount was the annual total of precipitation divided by 365 days. The intra-annual patterns described above are not captured in the annual totals.

Global Ecosystem Simulation System (GESSys)

Daily T_{max}, T_{min}, and precipitation for each 1° latitude by 1° longitude grid cell were used to estimate the other climatic inputs required by BIOME-BGC, using the model Climate Simulator (CLIMSIM) (Figure 2), based on the logic of Running et al. [1987] and Glassy and Running [1994]. Atmospheric transmittance was based on elevation and the difference between T_{max} and T_{min}, and rh was determined from T_{min}. For atmospheric pressure, elevation data were obtained at a resolution of 10 arc min from the U.S. Navy Fleet Numerical Oceanographic Data Center [Cuming and Hawkins, 1981; Kineman and Ohrenschall, 1992]. The 10 arc min data were averaged to obtain elevations at a resolution of 1° latitude by 1° longitude.

The Global Ecosystem Simulation System, GESSys, was used to handle the inputs and outputs of BIOME-BGC (Figure 2). For each grid cell, 2 years were simulated using the 1987 climatic data, the first year with initial soil water content set to full capacity, snowpack set to zero, and initial soil temperature set by latitude. The year-end values were used to start the second year. All carbon pools, including the M_{lit} and M_{soil}, were restored to their initial values. The daily outputs of NPP and R_h for the second year were saved for input to the atmospheric transport model.

Diagnostic NDVI Model

To provide an assessment of the seasonal and spatial patterns of the BIOME-BGC simulations, we calculated NPP and R_h using the diagnostic NDVI model presented in Heimann and Keeling [1989]. This model relies on the simplifying assumptions that the NPP flux is strictly proportional to PAR intercepted by the plant canopy and that R_h is a function only of air temperature. It does not explicitly account for water stress in plants or soil organisms. The diagnostic NDVI model provides a basis for comparison with the results of the process-based BIOME-BGC model both seasonally and spatially.

As we are trying to simulate the conditions for 1987 only, we regridded the 1987 biweekly NDVI data of Gallo [1992] to 1° by 1° cells. For PAR, we used the global data set for 1987 of Pinker et al. [1995], produced by inference from International Satellite Cloud Climatology Project C 1 satellite data with a spectrally resolved radiative transfer model [Pinker and Laszlo, 1992]. These data were provided as monthly averages on a 2.5° by 2.5° grid and contained a small number of missing monthly values in winter at high latitudes in both hemispheres. We estimated missing values by linear interpolation, for 1 or 2 consecutive months, or by an annual harmonic fit, for 3 to 6 consecutive missing months. We regridded the data to 1° by 1° cells, conserving the areal monthly intregral of PAR. Finally, R_h was calculated using the 1987 temperature data set of Piper [1995].

This model was tuned as in the work of Heimann and Keeling [1989] to give good correspondence to observations of atmospheric CO_2 for three stations (Point Barrow, Alaska; La Jolla, California; and Cape Kumukahi, Hawaii). Tuning produced an efficiency factor of 1.1 g C per MJ of intercepted PAR and an effective Q_{10} of 1.3.

Atmospheric Transport Model

Transport Model Description

The three-dimensional atmospheric Transport Model version 2 (TM2), used in the present study, is described by Heimann [1995]. It has a horizontal grid of 7.83° latitude by 10° longitude, 9 layers

Table 6. Net Annual Carbon Fluxes by Land Cover Type

Land Cover Type	NPP, Pg C	R_h, Pg C	NEE, Pg C
C_3 grassland	9.6	10.7	-1.1
C_4 grassland	8.0	11.9	-3.9
Evergreen needleleaf	6.6	5.8	0.8
Deciduous needleleaf	0.5	0.3	0.2
Evergreen broadleaf	17.5	22.4	-4.9
Deciduous broadleaf	4.6	5.8	-1.2
Shrubland	5.2	8.7	-3.4
Totals	52.0	65.6	-13.6

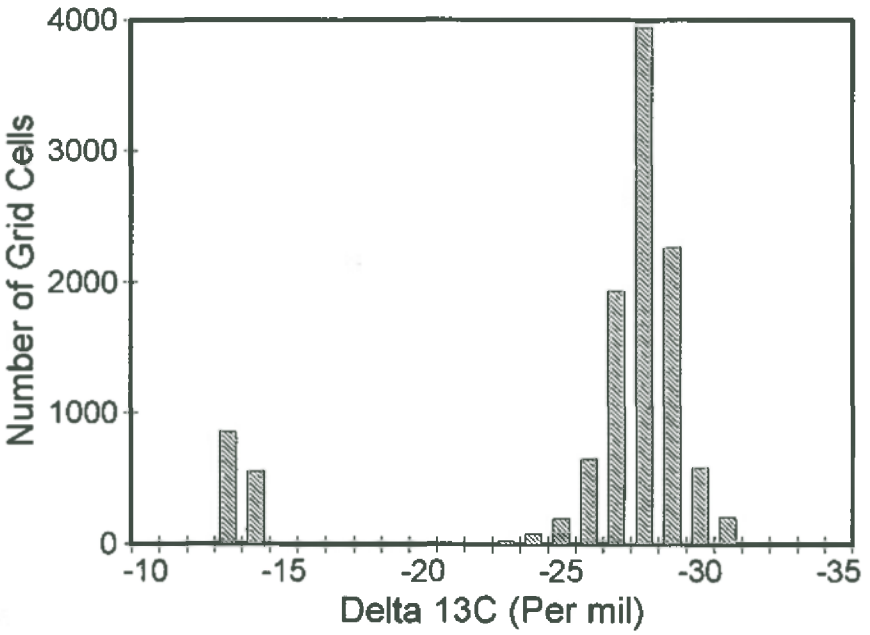

Figure 3. Frequency of occurrence of the carbon isotopic ratios, $\delta^{13}C$ (per mil) for each grid cell (1° latitude by 1° longitude). The two peaks are for C_4 photosynthetic and C_3 photosynthetic vegetation, respectively.

in the vertical dimension, and a numerical time step of 4 hours. There is no explicit planetary boundary layer (PBL) in the model. TM2 predictions of the seasonal CO_2 concentrations were well within the range of predictions from 10 other atmospheric transport models in the tracer transport model intercomparison project, TRANSCOM (R. W. Law et al., Variations in modelled atmospheric transport of carbon dioxide and consequences for CO_2 inversions, submitted to *Global Biogeochemical Cycles*, 1996). TM2 predicted a mean annual CO_2 north-south gradient similar to other models without an explicit PBL, the mean annual gradient was much smaller than models with an explicit PBL. Denning et al. [1995] shows that one explanation for the larger gradient is a correlation of the seasonal PBL depth with seasonal biospheric sources.

For this study, we have used wind fields for the year, 1987, which are based on meteorological observations processed by the four-dimensional assimilation system of the European Center for Medium-Range Weather Forecasts (ECMWF). For simulations of the atmospheric CO_2 concentration, TM2 was run by cycling over the model year, with the atmospheric motion repeated, for 4 years. The daily time series produced by the model for the fourth year were subsequently linearly detrended and Fourier transformed in order to obtain the coefficients of the first four harmonics constituting the seasonal variation at each station location.

Processing of NPP and R_h From BIOME-BGC

Daily predictions of NPP and R_h from the BIOME-BGC model were regridded from the 1° by 1° grid cells to 7.83° by 10° grid cells for input to TM2. Because (1) the annual totals of NPP and R_h in nature are approximately equal over the year, (2) we are focusing on the seasonal cycle of atmospheric CO_2, and (3) we have more confidence in the NPP than in the R_h predictions, we have chosen to adjust the annual soil respiration for each grid cell to equal the annual NPP, by using a simple multiplier to adjust the daily R_h. For the 1° by 1° cells in which the annual NPP is negative, we set daily fluxes for both NPP and R_h to zero.

Atmospheric Model Sources

Observations of atmospheric CO_2 were obtained from an array of land-based stations which lie approximately on a north-south line within the Pacific Ocean basin from the Arctic Ocean to the south pole (Table 5). All station data have been decomposed into a seasonal cycle, consisting of four harmonics, as described by Keeling et al. [1989a], and a linear trend.

In the northern middle to high latitudes, the terrestrial biosphere accounts for nearly the entire atmospheric CO_2 seasonal signal [Fung et al., 1987; Heimann et al., 1989]. However, farther south, as the fraction of land surface decreases, CO_2 fluxes associated with the oceans and with fossil fuel emissions become proportionally more important to the full seasonal signal. Therefore we have performed transport model simulations for five additional sources and sinks previously described by Heimann and Keeling [1989], Heimann et al. [1989], and Keeling et al. [1989b]. One of these, the seasonal air-sea CO_2 exchange flux, is a natural flux that is variable over the annual cycle. Three others are assumed constant over the annual cycle and contribute to the seasonal cycle only because of seasonally varying atmospheric transport. These are equatorial outgassing balanced by poleward oceanic uptake, North Atlantic Ocean uptake balanced by outgassing in the southern oceans, and industrial CO_2 emissions from fossil fuel combustion and cement manufacture. We have increased the industrial CO_2 emissions to the 1987 value of 5.7 Pg C per year [Andres et al., 1995] and have increased the corresponding ocean perturbation flux proportionally to 2.4 Pg C per year, from the 5.3 and 2.2 Pg C per year, respectively, given by Heimann and Keeling [1989]. The fifth source of CO_2 is a new

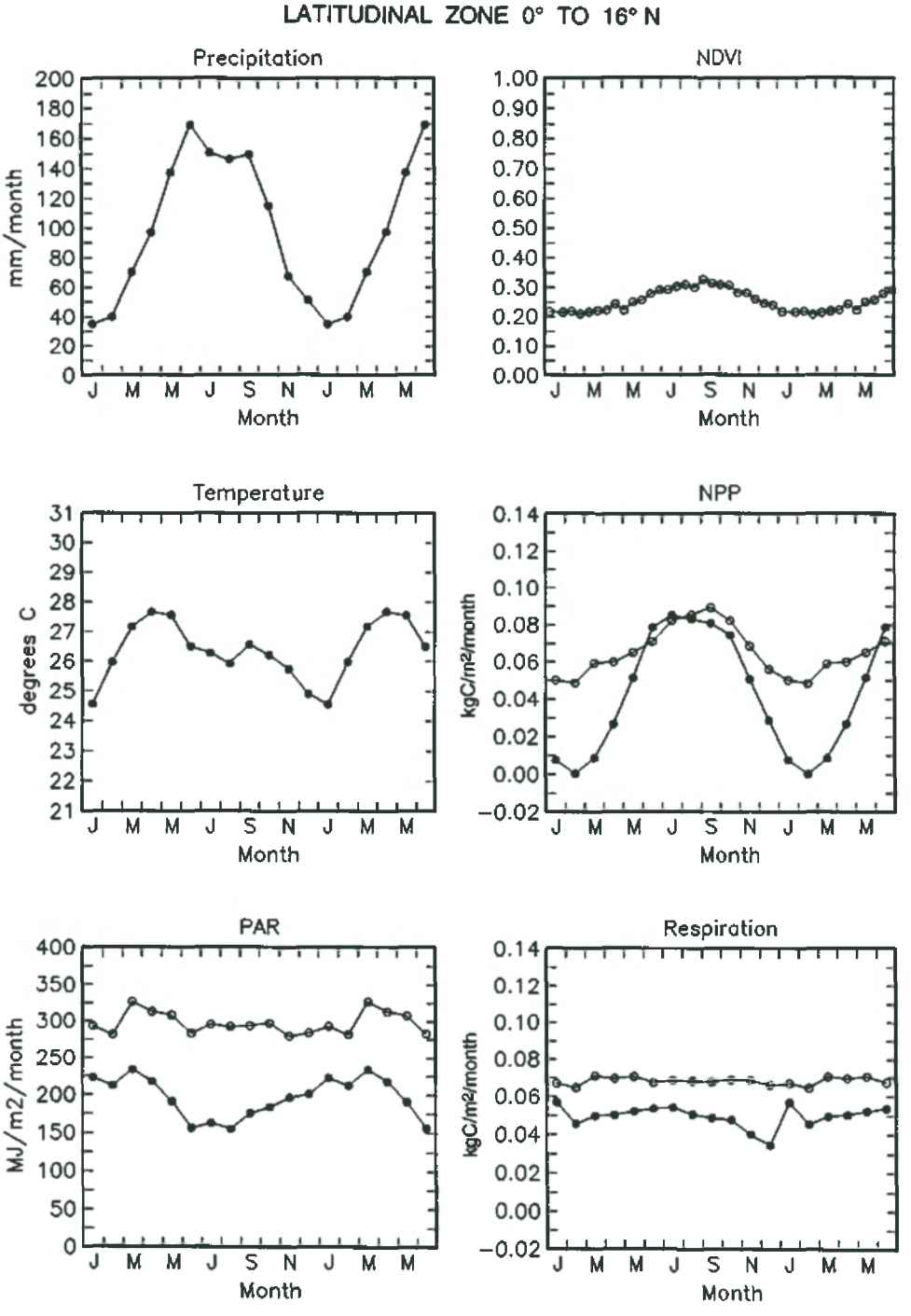

Figure 4a. Averages of the input parameters and output NPP and R_h for the BIOME-BGC and NDVI models for latitudinal zones in the northern hemisphere for 1987, for 0° to 16° N. For each latitudinal zone, area-weighted means have been calculated for daily precipitation and air temperature from Piper [1995], monthly photosynthetically active radiation from Pinker et al. [1995], biweekly normalized difference vegetative index (NDVI) from Gallo [1992], daily net primary production (NPP), and daily heterotrophic respiration (R_h). Only values pertaining to the 1° x 1° boxes employed in the BIOME-BGC model have been included. All quantities have been converted to monthly totals, except for temperature and NDVI, for which averages are shown. For PAR, NPP and R_h, the solid circles are for the BIOME-BGC; the open circles are for the diagnostic NDVI model. The first 6 months of the year 1987 are displayed twice to reveal the seasonal cycle more clearly.

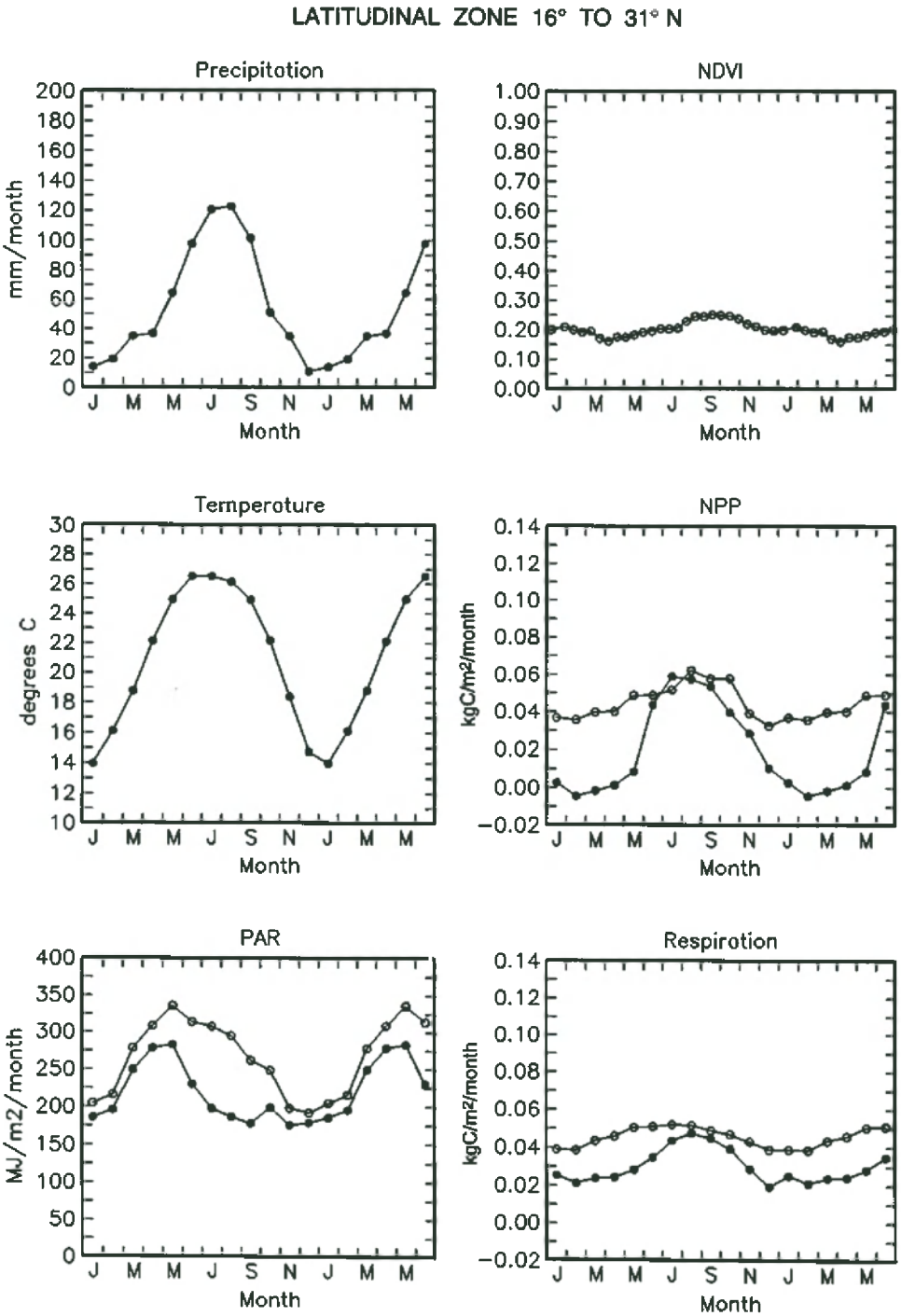

Figure 4b. Same as Figure 4a, except for 16° to 31°N latitude.

formulation for biomass burning (appendix B), which significantly influences the seasonality of atmospheric CO_2 in the tropics and the southern hemisphere.

Results

Global Carbon Fluxes

The global annual total of NPP for 1987 was simulated to be 52.0 Pg C y^{-1}, whereas the global R_h was simulated to be 65.6 Pg C y^{-1} (Table 6). Evergreen broadleaf forests, shrub lands and C_4 grasslands in tropical regions were net sources of carbon to the atmosphere, whereas needleleaf forests in the middle to high northern latitudes were net sinks of carbon. Not surprisingly, the areas with the highest LAI from the NDVI data (Plate 2 and Table 4) had the highest calculated annual totals of NPP (Plate 4 and Table 6). These areas are generally classified as evergreen needleleaf, evergreen broadleaf or deciduous broadleaf forests (Plate 2).

Annual NPP (Plate 4) was related to both annual precipitation

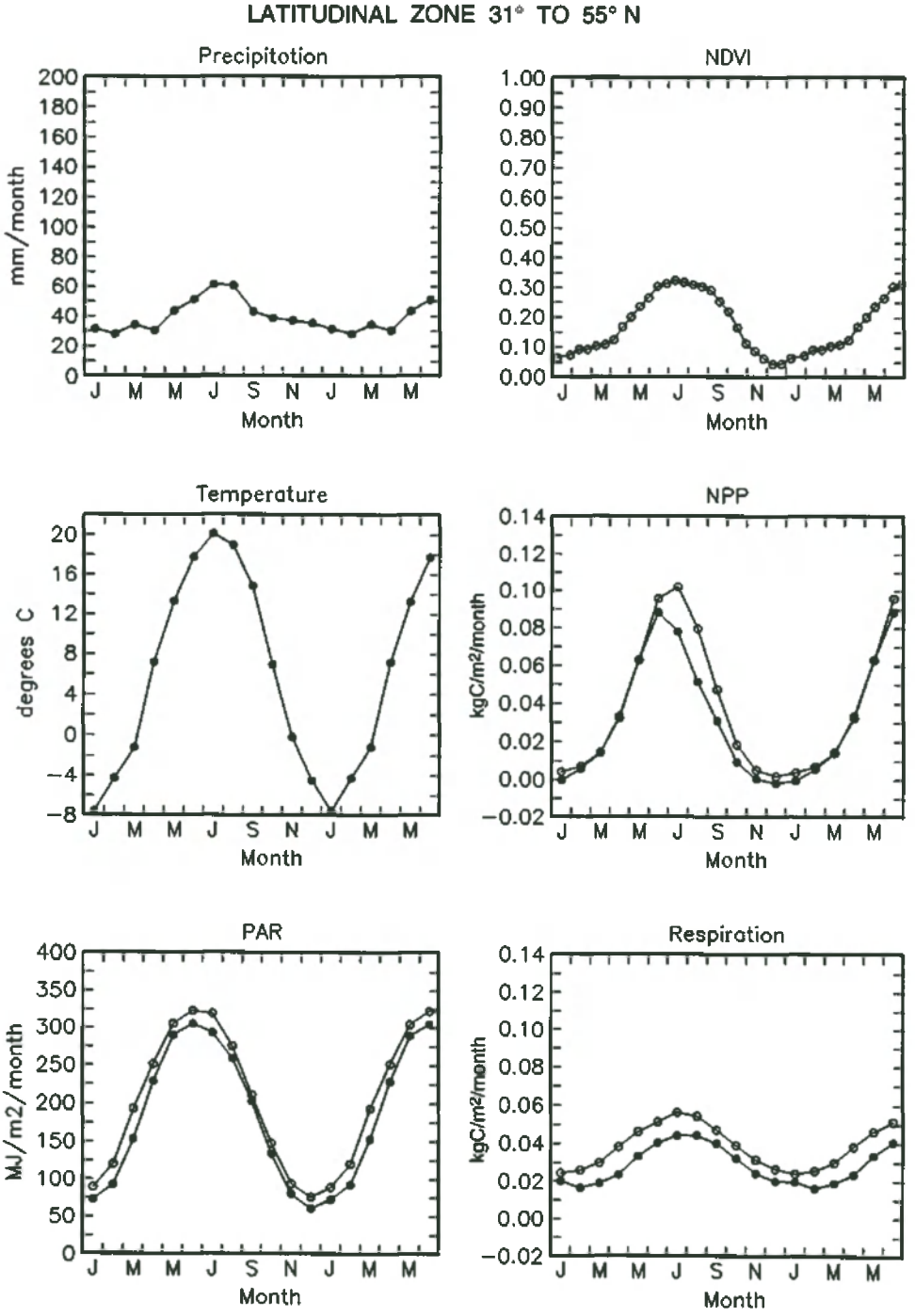

Figure 4c. Same as Figure 4a, except for 31° to 55°N latitude.

and LAI, with precipitation being the dominant factor in the tropical and subtropical latitudes (Plate 4) and LAI being dominant in the boreal latitudes (Plate 2). In error, some grid cells exhibited negative annual NPP, occurring mainly in the Indian subcontinent, southern Mexico, and the arctic tundra. We do not have a complete explanation for the negative NPP (Plate 4), although we suspect errors in model logic as the negative NPP occurs in ecosystems where the BIOME-BGC model was not tested. We also note that in two areas exhibiting negative NPP, the western United States of America and India, both experienced abnormally low precipitation in spring and summer in 1987. Negative NPP values in these areas may reflect an oversensitivity of NPP to water stress in the BIOME-BGC model.

The estimate of global NPP is consistent with other estimates [Potter et al., 1993; Melillo et al., 1993], as each of these models was calibrated to give answers within an acceptable range. Melillo et al.'s model is based on the hypothesis that nitrogen uptake controls NPP, whereas Potter et al.'s model assumes that absorbed radiation controls NPP. BIOME-BGC assumes that the primary control on NPP is the hydrologic budget. The fact that all models

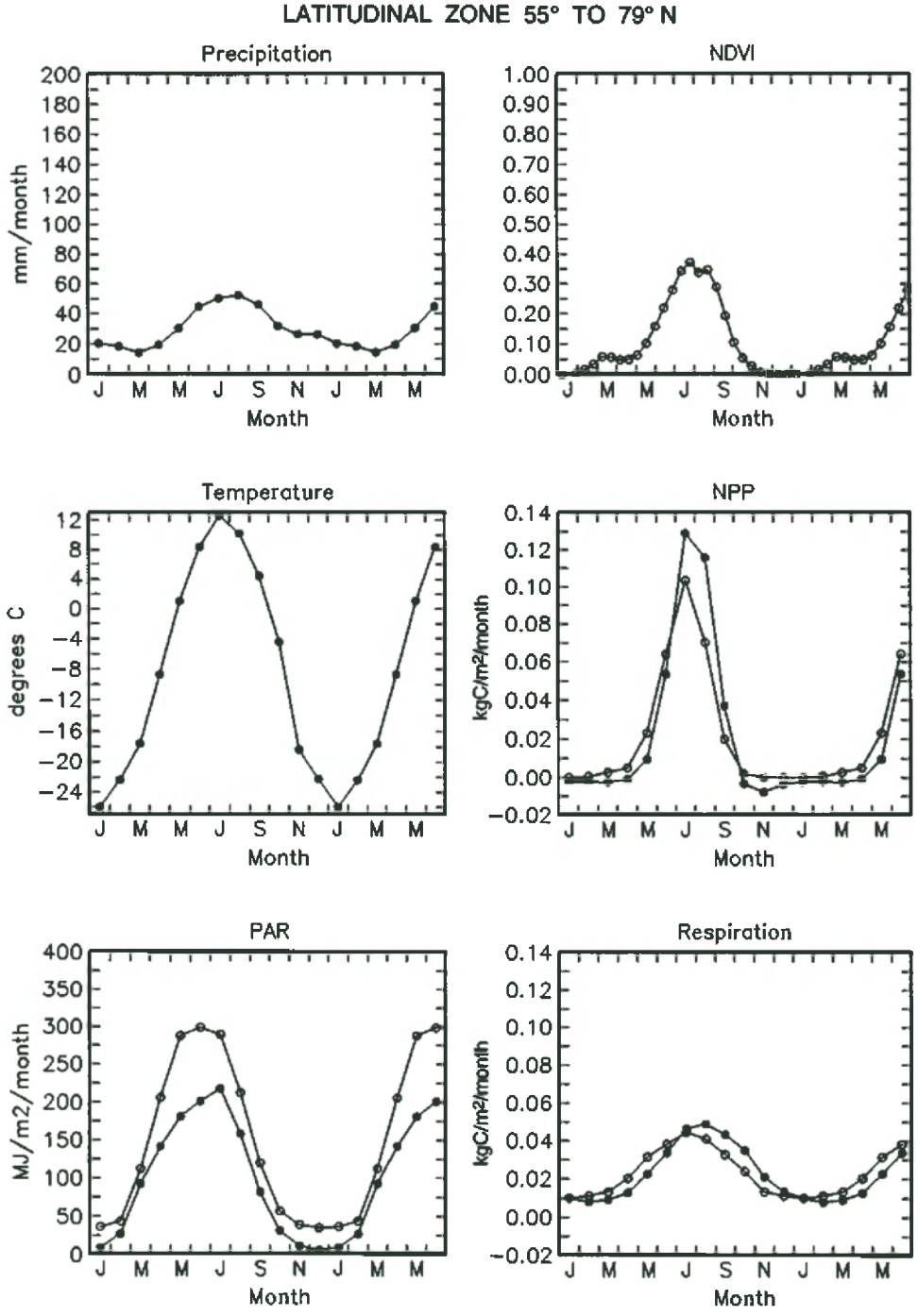

Figure 4d. Same a Figure 4a, except for 55° to 79°N latitude.

estimate similar values of global NPP, within a range of 10 Pg C, suggests that NPP is colimited by precipitation, nitrogen mineralization, and radiation. Indeed, BIOME-BGC simulates all three limitations during the annual time step [Running and Gower, 1991]; we find that precipitation, nitrogen mineralization and radiation equally influence LAI and hence NPP at equilibrium (E. R. Hunt, Jr. and S. W. Running, unpublished results, 1995]. Thus any of these controls will suffice for estimation of NPP, assuming ecosystems are at steady state with respect to vegetation, climate and soils. However, many ecosystems may be in transient successional stages after some sort of disturbance, for example, land use changes, fires, and extreme weather episodes, so the steady state assumption is probably not valid.

Similar to NPP, R_h in our simulation is correlated with LAI (Plate 5) because we initialized the litter carbon content (M_{lit}) from LAI. Clearly, because the interaction between temperature and moisture affects soil carbon (M_{soil}) and M_{lit} [Parton et al., 1987], each region of the earth should have different initial values of M_{soil}

and M_{lit} and hence different R_h. In our simulations, the direct effect of precipitation on R_h is ambiguous, because areas with high annual precipitation (Plate 3) also have high LAI (Plate 2) and therefore have high initial M_{lit}.

The large simulated global imbalance between NPP and R_h (13.6 Pg, Table 6) can not be correct, because globally, NPP and R_h must balance within 2 Pg C on average over several years, given the current understanding of the global carbon cycle [Sundquist, 1993; Schimel, 1995]. There are no global data to suggest which of these two numbers is more nearly correct, as it is the net difference between NPP and R_h which affects atmospheric CO_2 concentrations. Raich and Schlesinger [1993] and Raich and Potter [1995] suggest that soil respiration (consisting of root growth and maintenance respiration, litter decomposition and soil carbon turnover) ranges from 66 to 76.5 Pg C. Whereas their numbers agree approximately with our simulated estimates of global R_h, they are not comparable to ours because root growth and maintenance respiration are included in their values and not in ours.

Regional disparities in net ecosystem exchange (NEE) (NEE = NPP - R_h) are very apparent (Plate 6). Some areas in tropical latitudes have a negative net carbon exchange (R_h greater than NPP), whereas middle to high northern latitudes have positive exchange. M_{soil} in our model is based on potential vegetation from Holdridge Life Zones, not on our estimate of actual land cover type from the Matthews' [1983] data set. Thus our estimates of R_h in agricultural areas from high M_{soil} are probably too high, because most agricultural soils have about 25% less soil carbon because of cultivation [Houghton, 1994; Schimel et al., 1994]. For our continuing work, we will use a multiyear simulation, with better land cover type classifications, which will insure equilibrium values of NPP and R_h.

We have greater confidence in our estimates of NPP compared to R_h, because the predicted $\delta^{13}C$ values of the vegetation (Figure 3) for both C_3 and C_4 vegetation are similar to measurements reviewed recently by Vogel [1993]. The δ^{13} C of vegetation depends strongly on the water use efficiency (PSN per H_2O transpired) of photosynthesis [Farquhar et al., 1989], so the ratio of daily photosynthesis (i.e., gross primary production) to transpiration in the model is close to being correct. At steady state, there cannot be more transpiration than precipitation for a grid cell. Therefore precipitation establishes the upper limit of transpiration, and with reasonable simulated values of $\delta^{13}C$, also establishes the upper limit of photosynthesis.

Analysis of Outputs

Preparatory to comparing the simulations of the seasonal cycle of atmospheric CO_2 in the BIOME-BGC model with atmospheric observations, we present time plots of the critical model input parameters of NDVI, temperature, precipitation, and PAR and the simulated NPP and R_h from both models (Figures 4a - 4d). Plots of the zonal averages distinguish the boreal-arctic region (north of 55°N) from the midlatitudes (north of 31°N) and from low latitudes. The latter region is split at 16°N into two zones to aid in comparing these plots with atmospheric CO_2 data in which the seasonality is quite different at Christmas Island, near the equator, than farther north near Hawaii. We have not shown plots for the southern hemisphere because no unique features appear there to distinguish the NDVI predictions from the BIOME-BGC predictions.

Since the global annual totals for NPP are larger for the diagnostic NDVI model (69 Pg C compared to 52 Pg C from the BIOME-BGC), some care is needed to discern the differences between the seasonal simulations by the two models. At high latitudes, according to the BIOME-BGC model, NPP has a considerably greater seasonal amplitude than the NDVI model (Figure 4d). At low latitudes, BIOME-BGC predicts considerably lower NPP during the dry season, which is not seen in the NDVI model simulations (Figure 4a). Because R_h does not decrease as much as NPP during the dry seasons, the seasonal cycle of atmospheric CO_2 is the result of large seasonal changes in simulated NPP.

The zonal plots show good agreement between PAR derived from satellite data and as computed from surface temperature and precipitation data in midlatitudes (Figure 4c). This is understandable because the algorithm for estimating PAR from daily T_{max}, T_{min}, and precipitation was first developed for this region. We compared predicted NPP for each 7.83° by 10° grid cell which had at least 25% land; where the difference in NPP was 50% or greater, we examined the input data for clues as to the cause of the difference (Table 7). There was a clear reduction in PAR (and solar radiation) estimated by the Climate Simulator model for grid cells with 25% to 50% land cover probably because of a strong maritime influence. However, as PAR is near saturation for photosynthesis at the estimated LAI's, only 13 of 256 grid cells had significantly reduced NPP compared to the diagnostic NDVI model because of reduced PAR (Table 7).

The phenology algorithm in BIOME-BGC allowed 21 grid cells to start before and finish after the growing season as indicated by the diagnostic NDVI model (Table 7). These grid cells were generally assigned to C_3 grasslands in the northern hemisphere. Possibly, these grid cells are dominated by agriculture, in which the planting and harvesting dates are chosen to avoid frost damage. There were also 18 grid cells for which we could not assign possible causes for differences between the BIOME-BGC simulations and the diagnostic NDVI model simulations (Table 7). If these 18 grid cells were included with the grid cells that had errors attributed to both PAR from CLIMSIM and phenology from BIOME-BGC, then 80% of the 7.83° by 10° grid cells were reasonably well simulated by BIOME-BGC compared to the diagnostic NDVI model.

There were 27 grid cells in which the diagnostic NDVI model simulated high NPP when the monthly precipitation was very low, and presumably, photosynthetic rates were inhibited by drought stress (Table 7). This is not surprising as we have recognized that simple NDVI models require a term for drought stress [Running and Nemani, 1988; Nemani and Running, 1989b; Hunt and

Table 7. Preliminary Assignment of Model Errors

	Number of Grid Cells[a]
BIOME-BGC limiting PAR	13
BIOME-BGC long-growing season	21
Unknown errors	18
Total	52
Diagnostic NDVI model and precipitation	27
Total land grid cells[b]	256
Total globe grid cells	864

[a] Size is 7.83° latitude by 10° longitude.
[b] Grid cells with 25% or more land surface area.

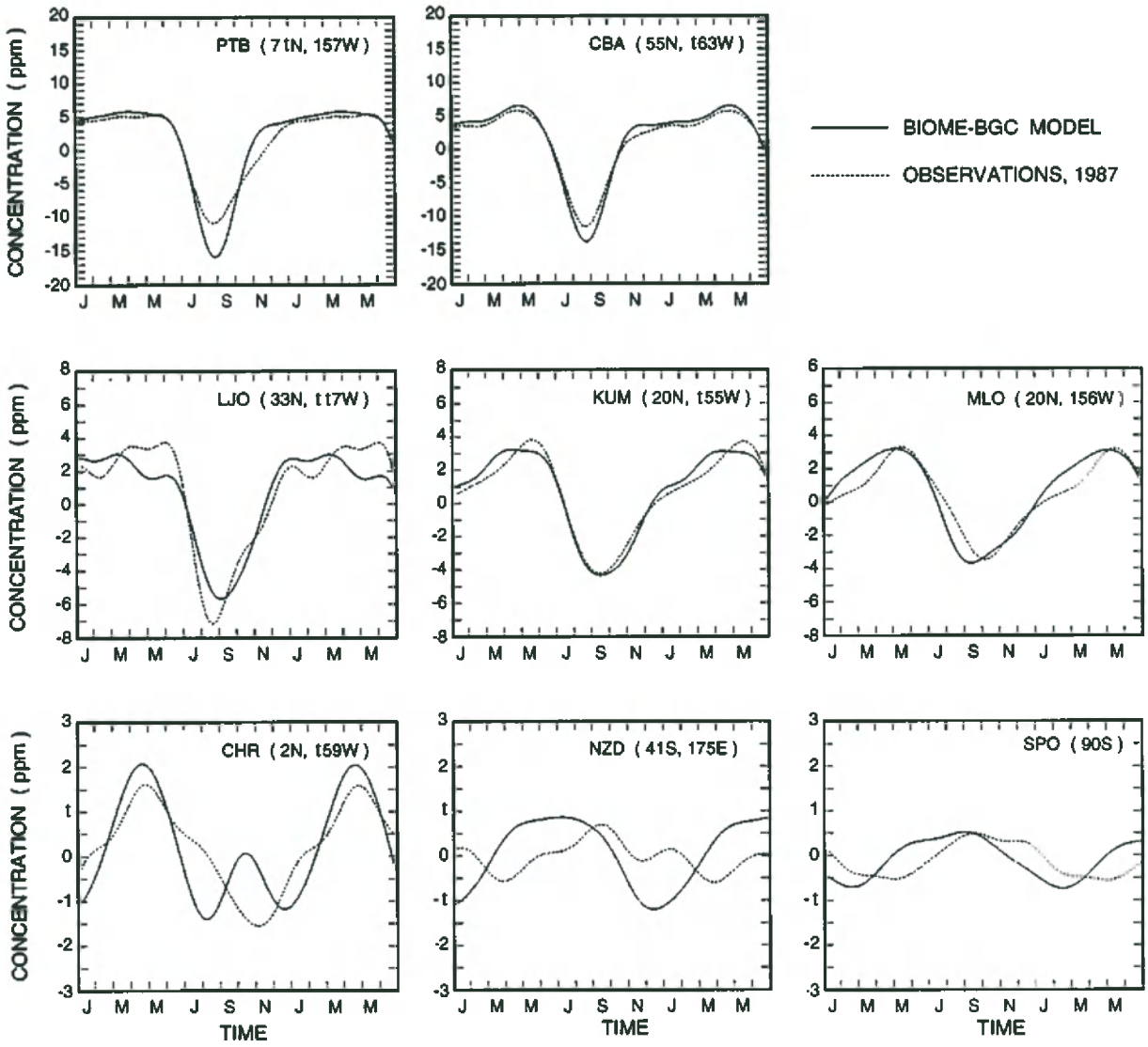

Figure 5. Seasonal variation of atmospheric CO_2, in ppm, for 1987 simulated by the BIOME-BGC model and compared to the observed variation at Point Barrow, Alaska (PTB); Cold Bay, Alaska (CBA); La Jolla, California (LJO); Cape Kumukahi, Hawaii (KUM); Mauna Loa, Hawaii (MLO); Christmas Island (CHR); Baring Head, New Zealand (NZD); and the south pole (SPO). Model and observational concentrations are represented by a sum of four harmonics fitted to the daily model predictions and to the individual observations. The model simulations are depicted by solid lines, the observations are depicted by dashed lines. The model simulations include variations resulting from the NPP and R_h produced by the BIOME-BGC model, from industrial CO_2 emissions, ocean sources and sinks, and from tropical biomass burning.

Running, 1992b]. Also, for high northern latitudes, low solar angles and partial snow cover may reduce NDVI of evergreen conifers during the early part of the growing season [Running and Nemani, 1988], so here NPP may be underestimated by the diagnostic NDVI model.

Comparison With Atmospheric CO_2 Observations

Comparisons of the BIOME-BGC model output with atmospheric CO_2 observations for 1987 are shown in Figure 5, and comparisons of the diagnostic NDVI model with atmospheric CO_2 observations are shown in Figure 6. Because the NDVI model is tuned to give optimal agreement at three stations (Point Barrow, Alaska; La Jolla, California; and Cape Kumukahi, Hawaii), only relative discrepancies between model simulations and observations at different latitudes are significant.

Two stations in Alaska, Point Barrow at 71°N and Cold Bay at 55°N, depict the seasonal cycle of CO_2 at high latitudes. The seasonal cycle composited from the BIOME-BGC shows a larger peak-to-peak amplitude than the observations for both stations while the NDVI model shows near agreement (Figures 5 and 6). Thus, the BIOME-BGC model shows a stronger seasonal cycle in the far north compared to the expectations from NDVI data. From the panels in Figure 4d for NPP and R_h for 55° to 79°N, it is apparent that this stronger cycle is a result of a stronger seasonality in NPP rather than a smaller seasonality in R_h. The phasing of

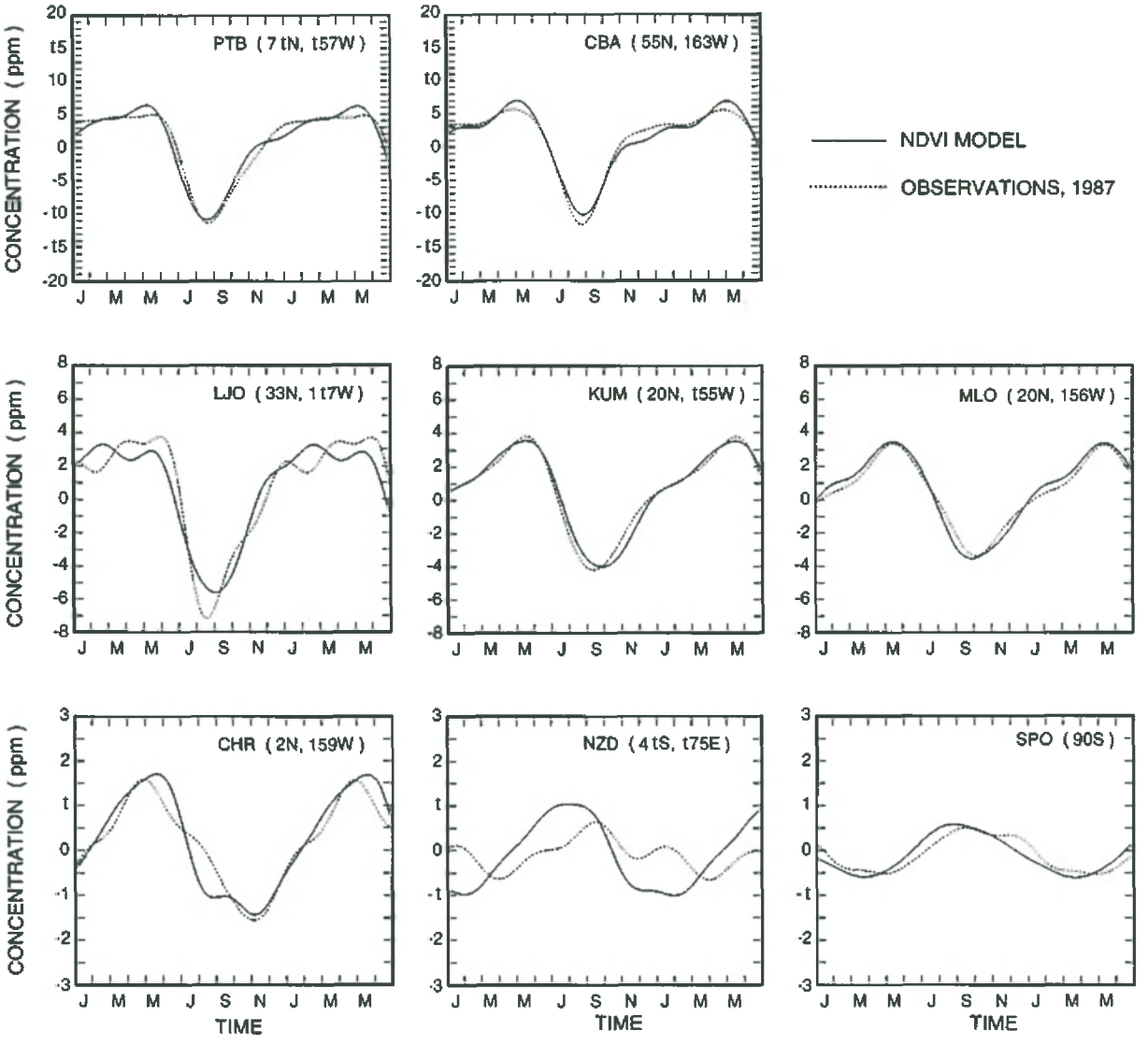

Figure 6. Same as Figure 13, except that the model simulations of NPP and R_h are by the diagnostic NDVI model.

both model simulations is in good agreement with the observations.

At La Jolla, California, both models show similar seasonal amplitudes, but both amplitudes are somewhat smaller than seen in the observations, in spite of the NDVI model having included this station in its tuning to the atmospheric CO_2 data (Figures 5 and 6). Air samples were taken only during periods with westerly winds off the Pacific Ocean to avoid contamination from nearby sources on land, whereas TM2 predicts CO_2 concentrations for all times. This sampling bias at least partially explains the phase differences between the predicted and observed CO_2 concentrations.

For two stations in Hawaii, Mauna Loa at an elevation of 3400 m above sea level and Cape Kumukahi, a coastal station, the agreement of both model composites with the data is close (Figures 5 and 6). Detailed examination for Cape Kumukahi indicates that the BIOME-BGC model predictions for the end of the season are advanced by about 10 days relative to the NDVI model. The phase advance for the end of the summer predicted by the BIOME-BGC model, consistent with the observations but not predicted by the diagnostic NDVI model, may be attributed to late season water stress when photosynthetic activity is restricted and the vegetation is still green [Running and Nemani, 1988].

For the station at Christmas Island, near the Equator but still within the northern hemisphere, the NDVI model simulation shows good agreement with the data, taking note of the much smaller seasonal cycle than farther north (Figure 6). This agreement is in spite of a relatively much larger contribution to the seasonal cycle from fossil fuel combustion and oceanic CO_2 exchange, as shown by earlier simulations at nearby Fanning Island [Heimann et al., 1989], and without this station being included in the tuning of the NDVI model. The BIOME-BGC simulation is unsatisfactory because of having a second seasonal component with a peak in October, which reflects seasonality of the tropics in the southern hemisphere (Figure 5).

Comparison of NPP simulations for the zones from the equator to 31°N indicate that the BIOME-BGC model shows strong seasonality in net ecosystem exchange, because of changes in NPP not reflected by NDVI (Figures 4a and 4b). Some tropical ecosystems continue to assimilate CO_2 during the dry season

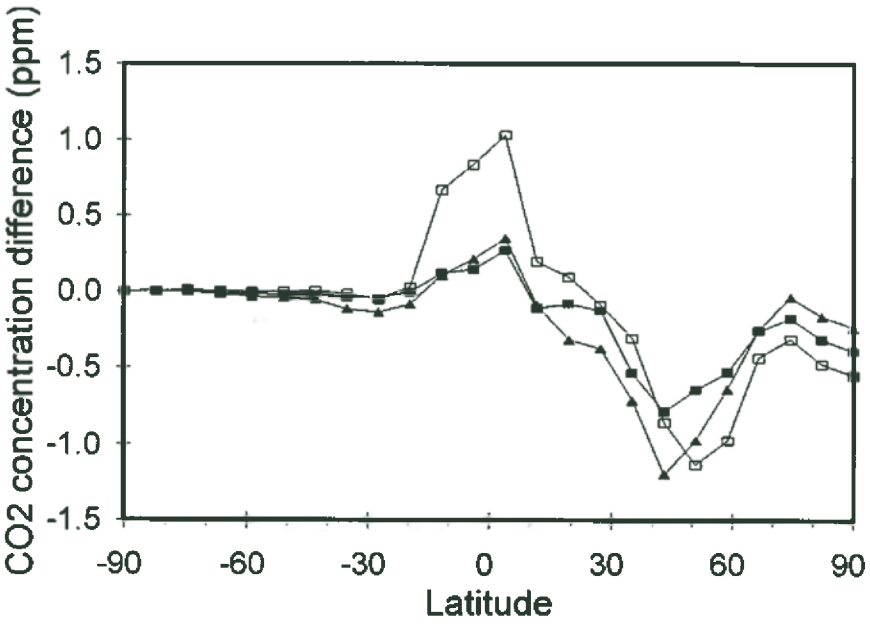

Figure 7. Surface, zonally averaged, mean annual CO_2 concentrations simulated by the atmospheric transport model (TM2) with 1987 winds expressed as a difference from the mean of the south pole. The net sources from Fung et al. [1987] (solid squares) were linearly interpolated between the midpoints of each month and were regridded to 7.83° by 10° grid cells, to show as a comparison to the BIOME-BGC (open squares) and diagnostic NDVI model outputs (triangles) from the TM2 model.

sufficient to balance total respiration, drawing up water from 8 m or more [Nepstad et al. 1994].

At Baring Head, New Zealand at 41°S, both BIOME-BGC and the diagnostic NDVI models predict nearly the same seasonality, but neither prediction is close to agreement with the observations. The agreement with observations is better for the south pole, but still not satisfactory. Here the oceanic contributions to the seasonal cycle are as large as the terrestrial ecosystem fluxes and the atmospheric transport from the tropics and northern hemisphere. Biomass burning contributions are a smaller but significant component of the seasonal cycle. Hence more work is required in understanding the seasonality of the atmospheric CO_2 observations.

Latitudinal Profiles of Mean Annual CO_2 Concentrations

Although seasonal NPP and R_h are balanced for each grid cell to give a zero net annual flux, they covary with the seasonal atmospheric transport to produce nonzero annual mean concentrations [Fung et al., 1987; Keeling et al., 1989b; Denning et al., 1995]. In Figure 7, we show a comparison of the mean annual CO_2 concentrations for different latitudinal zones using the net carbon fluxes from Fung et al. [1987], BIOME-BGC, and the diagnostic NDVI model. The Fung et al. [1987] and the NDVI model inputs to the TM2 simulations agree reasonably well; the differences north of 10° latitude are attributable to the lower NPP of Fung et al. [1987] (47 Pg C compared to 61 Pg C global annual totals, respectively). All three models predict a local maximum in CO_2 concentrations in the tropics (Figure 7); however, net fluxes from BIOME-BGC cause the annual mean to be 0.7 ppm higher than the other two models. This difference is from the differences in NPP compared to R_h because of greater seasonality (Figures 4a and 4b).

Discussion

This paper describes a comprehensive, global-scale, ecosystem process model driven by external forces which control the assimilation, respiration, and storage of carbon on timescales from a few days to several decades. Atmospheric CO_2 measurements provide evidence of how these processes vary over this entire range of timescales. With the necessary input data: NDVI, temperature, precipitation, solar radiation, and initial soil and land cover conditions, this model should therefore simulate the variations in atmospheric CO_2 that have been observed since precise measurements began in 1958. At present, suitable global climatic data are only available from 1977 to the present, but even this shorter time span allows a wide range of events in the carbon cycle to be examined, including the El Niño event of 1982-1983 and a recent slow down in the rate of rise of atmospheric CO_2 from 1989 to 1993 [Keeling et al., 1995].

The challenge of scaling up elements of our model to produce global scale predictions has been formidable. Also, much of the input information we desire, such as gridded daily climatic data, had to be assembled from databases inadequate for the task, even though these databases were the best available when we started this study. Remote sensing data from satellites have supplemented our information from ground-based studies, especially in providing indices of terrestrial vegetation worldwide, but remotely sensed data also have shortcomings, such as inadequate long-term calibrations. We note that considerable effort is being made by the scientific community to update and improve these required databases [Sellers et al., 1996].

BIOME-BGC and other terrestrial ecosystem process models are first tested with site-specific data on homogeneous plots of representative ecosystems. At these small scales, numerous data exist to both parameterize and test model outputs. Often,

unmeasurable parameters are adjusted to match the results of a specific study on a single site, and the reasonableness of these parameters is then tested with other site-specific data. There are simply too few sites with sufficient data of the necessary kind to test ecosystem models at global scales. Similar processes, such as NPP, from different ecosystems are measured by different methods, each of which introduces errors. Further experimental investigations at different homogeneous sites, worldwide, would improve understanding of ecosystem processes encapsulated by simulation models, but they would not be necessarily applicable to these same processes at the global scale because these homogeneous sites may not be truly representative.

With both satellite and ground-based information, we have constructed a global scale biospheric model which predicts plant activity on a daily basis, using as much as possible, the actual conditions during 1987. Thus the outputs of these simulations allow comparison with atmospheric CO_2 data at an array of stations from the Arctic to the south pole, which can be used to assess the model's logic, the key objective of this study. Of particular interest in this respect is the magnitude of the drawdown of CO_2 from the atmosphere during the spring to fall growing season, which atmospheric CO_2 data provide with considerable regional detail. The model, to be valid, should reproduce this drawdown with a close approximation to both amplitude and phase. We have refrained from adjusting the BIOME-BGC model deliberately to match better the data, because the terrestrial biosphere model has many more degrees of freedom compared to atmospheric CO_2 observations. The atmospheric CO_2 data provide a means to prove models wrong but not to prove them unambiguously correct.

With respect to the fate of CO_2 produced by the combustion of fossil fuels, the atmospheric data should provide an accurate estimate of the global imbalance in the carbon cycle from year to year. Isotopic measurements of the $^{13}C/^{12}C$ ratio of atmospheric CO_2 permit the terrestrial contribution of this imbalance to be determined for timescales approaching a decade [Keeling et al., 1989a], again with some regional detail. These data will eventually provide a second, independent data set for model assessment.

The simulation of atmospheric CO_2 based on satellite-derived NDVI data, when tuned by global adjustment of the relation of NPP to NDVI and of the temperature sensitivity of soil respiration, gives better agreement with the observations than the BIOME-BGC model in its present formulation. The agreement of CO_2 observations with NDVI data, with full knowledge of the deficiencies of the NDVI model, allows assessment of any process model, with the likelihood that NDVI model predictions provide insight as to possible misrepresentations by the process model. This is supported by the general agreement of two different NDVI models in calculating the annual means of atmospheric CO_2 concentrations for different latitudinal zones.

There were four areas where comparisons of BIOME-BGC, the diagnostic NDVI model, and the TM2 transport model of atmospheric CO_2 showed how each of the models may be improved. First, the annual total of NPP in the tropical latitudes was underestimated and the seasonality of NPP in the high northern latitudes was overestimated by BIOME-BGC, in comparison with both the NDVI diagnostic model and atmospheric CO_2 observations. BIOME-BGC and the$_2$ CO observations indicated that vegetation during late summer were drought-stressed in the middle northern latitudes, which was not consistent with the NDVI model. Finally, the oceanic CO_2 fluxes or TM2 model transport may be in error, leading to poor agreement of simulations with observations in the southern hemisphere, in spite of the good agreement between BIOME-BGC and the diagnostic NDVI model simulations.

The solution that we presented in this study is to test ecosystem models at global scales with data for carbon isotopes, temporal NDVI, and atmospheric CO_2. Carbon isotope data are available worldwide; however measurements of $\delta^{13}C$ of vegetation depend on knowing the $\delta^{13}C$ of the atmosphere, so these data can provide only relative agreements between NPP and precipitation. The diagnostic NDVI model is spatially and temporally explicit thereby encompassing the range of vegetation heterogeneity at regional and global scales. The atmospheric CO_2 station data provide seasonal estimates of net ecosystem exchange (NEE), the difference between NPP and R_h, for large regions over the globe. This top-down approach complements methods of model assessment using homogeneous plot data. By further development and testing of these combined models, we believe we can estimate the responses of terrestrial ecosystems to the interannual variability of climate that are hypothesized from studies on the anomalies of the global atmospheric CO_2 data.

Notation

A_{max}	maximum rate of photosynthesis (μmol m^{-2} s^{-1}).
A_m	maximum rate of photosynthesis corrected for air temperature (μmol m^{-2} s^{-1}).
A_n	LAI-averaged photosynthetic rate at solar noon (mol m^{-2} s^{-1}).
a	albedo (dimensionless).
C_a	ambient CO_2 partial pressure (Pa).
C_i	intercellular CO_2 partial pressure (Pa).
c_p	heat capacity of air (J kg^{-1} $°C^{-1}$).
D	vapor pressure deficit between leaf and the free atmosphere (kPa).
d_s	soil depth (m).
d_t	declination (degrees).
E_{can}	evaporation from the canopy (m^3 H_2O m^{-2} s^{-1}).
E_{soil}	evaporation from the soil (m^3 H_2O m^{-2} s^{-1}).
$e_s(T)$	saturated vapor pressure of air at temperature T (Pa).
ET	evapotranspiration (m^3 H_2O ha^{-1} day^{-1}).
f_s	ratio of sapwood cross-sectional area to leaf area (cm^2 m^{-2}).
G	growth respiration (kg C ha^{-1} d^{-1}) for leaves (lf), stems (st), coarse roots (cr), and fine roots (fr)(G_{lf}, G_{st}, G_{cr}, and G_{fr}, respectively).
g	fraction of photosynthesis for growth respiration of leaves (lf), stems (st), coarse roots (cr), and fine roots (fr)(g_{lf}, g_{st}, g_{cr}, and g_{fr}, respectively).
g_b	boundary-layer conductance of H_2O (mm s^{-1}).
g_c	stomatal conductance to CO_2 (mol m^{-2} s^{-1}).
g_{max}	maximum stomatal conductance of H_2O (mm s^{-1}).
g_m	canopy-average, daily-average stomatal conductance (mm s^{-1}).
g_c	total canopy stomatal conductance of H_2O (mm s^{-1}).
g_{soil}	soil surface conductance of H_2O (mm s^{-1}).
h	forest canopy height (m).
h_{max}	maximum forest canopy height (m).
k	extinction coefficient of canopy (LAI^{-1}).
L	leaf lignin mass to nitrogen mass (kg lignin per kg N).
LAI	leaf area index (m^2 m^{-2}).
LAI_{max}	maximum leaf area index determined by land cover type.

M carbon mass (kg C ha^{-1}) of leaves (lf), stems (st), coarse roots (cr), fine roots (fr), litter (lit), and soil (M_{lf}, M_{st}, M_{cr}, M_{fr}, M_{lit}, and M_{soil}, respectively).
NDVI normalized difference vegetation index (dimensionless).
NEE net ecosystem exchange (kg C ha^{-1} y^{-1} or kg C ha^{-2} d^{-1}).
NPP net primary production (kg C ha^{-1} y^{-1} or kg C ha^{-2} d^{-1}).
P atmospheric pressure (kPa) calculated from elevation.
PAR photosynthetically active radiation from 400 nm to 700 nm wavelength (μmol m^{-2} s^{-1}).
PSN net photosynthesis (kg C ha^{-1} d^{-1}, gross photosynthesis net daytime maintenance respiration of leaves.
Q_{10} exponential temperature response factor.
R respiration (kg C ha^{-1} d^{-1}) for leaves (lf), stems (st), coarse roots (cr), fine roots (fr), litter (lit), and soil (R_{lf}, R_{st}, R_{cr}, R_{fr}, R_{lit}, and R_{soil}, respectively).
R_a autotrophic respiration (kg C ha^{-1} d^{-1}).
R_h heterotrophic respiration (kg C ha^{-1} d^{-1}).
r specific rate of respiration (kg C kg^{-1} C d^{-1}) for leaves (lf), stems (st), coarse roots (cr), fine roots (fr), litter (lit), and soil (r_{lf}, r_{st}, r_{cr}, r_{fr}, r_{lit}, and r_{soil}, respectively).
^{13}R isotopic mass ratio of $^{13}C/^{12}C$.
$^{13}R_0$ isotopic mass ratio of the Pee Dee Belemnite standard.
rh relative humidity (%).
S_a canopy absorbed solar radiation (MJ m^{-2} d^{-1}).
S_0 daily solar radiation (MJ m^{-2} d^{-1}).
S_t canopy transmitted solar radiation (MJ m^{-2} d^{-1}).
s_v slope of saturated vapor pressure versus air temperature (Pa $°C^{-1}$).
SLA specific leaf area (m^2 kg^{-1} C).
t day of year.
T_{air} average daily air temperature (°C).
T_{day} daytime average air temperature (°C).
T_{max} maximum daily air temperature (°C).
T_{min} minimum daily air temperature (°C).
T_{night} nighttime average air temperature (°C).
T_{opt} optimum temperature for photosynthesis (°C).
T_{soil} average daily soil temperature at 0.1 m depth (°C).
W_{max} maximum soil water content (m^3 H_2O ha^{-1}).
W_{soil} soil water content (m^3 H_2O ha^{-1}).
α_g initial slope of stomatal conductance versus PAR ((mm s^{-1})/(μmol m^{-2} s^{-1})).
α_{max} maximum quantum yield (mol CO_2 mol^{-1} photons).
α_p quantum yield for photosynthesis (mol CO_2 mol^{-1} photons).
β_m temperature coefficient of maintenance respiration ($°C^{-1}$).
β_p temperature coefficient of photosynthesis ($°C^{-1}$).
β_s temperature coefficient of heterotrophic respiration ($°C^{-1}$).
γ psychrometric constant (Pa $°C^{-1}$).
Γ CO_2 compensation point of photosynthesis (Pa).
$\delta^{13}C$ ratio of $^{13}C/^{12}C$ compared to the standard ($^{13}R/^{13}R_0$-1).
Δ discrimination of $^{13}C/^{12}C$ from photosynthesis.
ϵ PAR conversion efficiency (kg C MJ^{-1} PAR).
η fractional allocation of photosynthesis for leaves (lf), stems (st), coarse roots (cr), and fine roots (fr) (η_{lf}, η_{st}, η_{cr}, and η_{fr}, respectively).
Θ volumetric water content of soil (m^3 m^{-3}).
Θ_{max} volumetric water content of soil at field capacity (m^3 m^{-3}).
λ latent heat of vaporization (J m^{-3}).
ξ fraction of daylight period at maximum photosynthesis.
ρ_{air} density of dry air (kg m^{-3}).
ρ_{wood} density of wood (kg C m^{-3}).
ς length of daily light period or "daylength" (s d^{-1}).
ς_{24} number of seconds in 24 hours (86,400 s).
ϕ latitude (degrees).
$\Psi_{predawn}$ predawn leaf water potential (MPa).
Ψ_{soil} soil water potential (MPa).
Ψ_{stress} leaf water potential at stomatal closure (MPa).

Appendix A: Description of BIOME-BGC

Climatic Inputs

The inputs from extant climatic data (Table 1) for a given day of the year are: T_{max}, T_{min}, and daily precipitation (mm H_2O d^{-1}). Some inputs which may either be from data or derived (Table 1) are rh, T_{soil}, S_0, and PAR. According to Gates [1980], ϕ and d_l are used to calculate ς or "day length:"

$$\varsigma = 480 \cos^{-1}(-\tan\phi \cdot \tan d_l) \quad \text{(A1)}$$

where 480 converts the half-day length to a full day given 240 s of time per degree longitude. T_{air} is taken to be the mean of T_{max} and T_{min}, whereas T_{day} and T_{night} are calculated:

$$T_{day} = 0.212\,(T_{max} - T_{air}) + T_{air} \quad \text{(A2)}$$

$$T_{night} = 0.5\,(T_{day} + T_{min}) \quad \text{(A3)}$$

from Running and Coughlan [1988]. D is

$$D = e_s(T_{day}) \cdot (1 - rh) \quad \text{(A4)}$$

T_{soil} is calculated from Zheng et al. [1993]:

$$T_{soil}(t) = T_{soil}(t - 1) + [T_{air}(t) - T_{soil}(t - 1)] \exp(-k\,LAI) \quad \text{(A5)}$$

with LAI slowing the rate of increase in T_{soil}.

S_a and S_t through the canopy are calculated using the Beer-Lambert law:

$$S_t = (1 - a)\,S_0 \exp(-k\,LAI) \quad \text{(A6)}$$

$$S_a = (1 - a)\,S_0\,(1 - \exp(-k\,LAI)) \quad \text{(A7)}$$

where a is set to 0.15 as a global average. The Beer-Lambert extinction coefficient k was assumed to be 0.5 for all land cover types on a one-sided leaf area basis, which is approximately the average for conifers and deciduous broadleaved trees [Jarvis and Leverenz, 1984] and for grasses [D. S. Schimel, personal communication, 1994].

Stomatal Conductance and the Hydrologic Budget

W_{max} is calculated from Θ_{max} multiplied by d_s and corrected for coarse fragment content and the number of square meters in 1 ha (10,000 m^2 ha^{-1}). Daily, W_{soil} is calculated from the net sum of the various hydrologic fluxes (Figure 1), then Θ is calculated from

W_{soil} and d. Soil texture and Θ are then used to calculate Ψ_{soil} [Saxton et al., 1986], which directly affects the vegetation.

Daily precipitation, when it occurs, is partitioned into either rain or snow depending on whether T_{night} is above or below 0°C, respectively. Snowmelt is determined from T_{day} and S_t [Coughlan and Running, 1996] and is added to W_{soil} (Figure 1). Rain is intercepted by the canopy until a maximum of 0.5 mm per one-sided LAI is achieved. Intercepted water is evaporated with a limit set by S_a. Rain not intercepted, or throughfall, is added to W_{soil}. If W_{soil} exceeds W_{max}, the excess is removed as outflow. E_{soil} is calculated from the Penman-Monteith equation:

$$E_{soil} = (s_v S_a/\varsigma + \rho_{air} c_p g_b D)/[\lambda(s_v + \gamma g_b/g_{soil})] \quad (A8)$$

where g_{soil} is the maximum g_{soil} divided by the square root of the number of days since rainfall [J. B. Stewart, personal communication, 1993]; maximum g_{soil} is set to be 2 mm s^{-1} as reported by Baldocchi and Meyers [1991]. Total daily soil evaporation (m^3 ha^{-1} d^{-1}) is equal to E_{soil} ς 10,000 m^2 ha^{-1}.

For each land cover type (Table 2), g_{max} is determined from the literature correcting for a bias of measuring young, healthy leaves. We applied the logic of Rastetter et al. [1992] for canopy-average photosynthetic rate for calculating g_m:

$$g_m = (g_{max}/k\ LAI) \cdot \ln\{(g_{max} + \alpha_g\ PAR)/$$

$$[g_{max} + \alpha_g\ PAR\ \exp(-k\ LAI)]\} \quad (A9)$$

Then a series of multipliers, $f(D)$, $f(\Psi_{soil})$, $f(T_{day})$, and $f(T_{min})$, all ranging from 0.0 to 1.0, are calculated for stomatal responses to D, Ψ_{soil}, T_{day}, and T_{min}, respectively [Running and Coughlan, 1988]. The multiplier $f(D)$ is equal to 1.0 when D is less than or equal to 7.5 kPa, is 0.0 when D is greater than or equal to the vapor pressure deficit causing stomatal closure (Table 2), and is linear between these two points. Using an equation from Rastetter et al. [1991], $f(T_{day})$ is

$$f(T_{day}) = \exp\{\ln[(45 - T_{day})/(45 - T_{opt})]\ \beta_p\ (45 - T_{opt})\}$$

$$\exp\{\beta_p\ (T_{day} - T_{opt})\} \quad (A10)$$

where 45°C is the maximum temperature and β_p is a temperature coefficient which we set to be 0.2 for vegetation with the C_3 pathway and 0.12 for vegetation with the C_4 pathway. The $f(\Psi_{soil})$ assumes $\Psi_{predawn}$ is -0.5 MPa when Ψ_{soil} is greater than -0.5 MPa, and $\Psi_{predawn}$ is equal to Ψ_{soil} when Ψ_{soil} is less than -0.5 MPa. Thus

$$f(\Psi_{soil}) = 1 - (-0.5 - \Psi_{predawn})/(-0.5 - \Psi_{stress}) \quad (A11)$$

where Ψ_{stress} is given in Table 2. Then

$$g_s = g_m\ f(D)\ f(\Psi_{soil})\ f(T_{day})\ f(T_{min})\ LAI \quad (A12)$$

because conductances in parallel are additive, multiplication by LAI is required for g_s. E_{can} is calculated using the Penman-Monteith equation:

$$E_{can} = (s_v S_a/\varsigma + \rho_{air} c_p g_a D)/\lambda(s_v + \gamma g_a/g_s) \quad (A13)$$

where g_a is assumed to be a constant for each land cover type (Table 2). Total daily transpiration is then calculated as E_{can} ς 10,000 m^2 ha^{-1}. ET is the sum of daily transpiration, evaporation from the soil, and evaporation of intercepted precipitation.

The leaves of deciduous forests and grasses, and the fine roots of all land cover types, have certain periods of the year when they are actively respiring. Coarse roots and stems respire year round, controlled by soil and air temperature, respectively. Leaves photosynthesize and transpire when they are green and active. For the fine roots of all land cover types, and for the leaves of the two grassland and shrub cover types, activity commences on a day of the year when conditions are favorable. We assume that favorable conditions occur when $\Psi_{soil} > -0.025$ MPa and $T_{soil} > 3$°C. When conditions are unfavorable, $\Psi_{soil} < \Psi_{stress}$ (Table 2) or $T_{soil} < -1$°C, activity ceases on that yearday and LAI is set to zero in the model. For the two land cover types of deciduous forest, leaf activity commences when an 11-day running average of previous $T_{min} > 3$°C and ceases when that running average of $T_{min} < -1$°C. Leaves for the two evergreen forest cover types are "active" at all times, however, rates of photosynthesis and transpiration are negligible during periods with low T_{min} or low Ψ_{soil}. These are our best guesses to explain the correlation of activity to degree days, which can not be extended in either space or time.

Photosynthesis and Stable Carbon Isotope Discrimination

For C_3 photosynthesis, a biochemical photosynthesis model based on the equations of Farquhar et al. [1980] and McMurtrie et al. [1992] is used to simulate A_{max} at the optimum temperature as a function of atmospheric CO_2 [Hunt and Running, 1992a]. As we are using 1987 data, with an average atmospheric CO_2 concentration of 347 ppm [Keeling et al., 1989a], we selected an A_{max} for each land cover type from data derived from numerous field studies (Table 2), again correcting for a bias of measuring the rates of younger leaves. Daily A_m is calculated:

$$A_m = A_{max}\ f(T_{min})\ f(\Psi_{soil}) \quad (A14)$$

For C_4 photosynthetic plants, α_p is simply set at 0.05, and for C_3 photosynthetic plants, α_p depends on T_{day} and C_i [Ehleringer and Björkman, 1977]:

$$\alpha_p = (\alpha_{max} - 0.0010\ T_{day})\ (C_i - \Gamma)/(C_i + 2\Gamma) \quad (A15)$$

where α_{max} is 0.0825 mol CO_2 per mole photons, C_i is initially estimated from A_m, and Γ is calculated from T_{day} and atmospheric O_2 concentration [Farquhar et al., 1980]. For solar noon, A_n is

$$A_n = (A_m/k\ LAI)\ \ln\{(A_m + \alpha_p\ PAR)/$$

$$[A_m + \alpha_p\ PAR\ \exp(-k\ LAI)]\} \quad (A16)$$

from Rastetter et al. [1992]. A_n must be integrated over the daylight period, so we assumed the instantaneous value of PAR varies from dawn to dusk as a sine curve, with the daylight period from 0° to 180°. We defined relative variables as the ratios of the instantaneous rates of A_n and PAR to their maximum values for the day, substituted these relative variables for A_m and PAR in equation (A16), and integrated this equation to determine ξ. The range of ξ for various values of A_m, LAI, k, and α_p was from 0.81 to 0.89; thus, we set ξ to be the median value, 0.85. PSN was calculated from A_n by converting moles of CO_2 to kilograms of carbon:

$$PSN = A_n \text{ LAI } \varsigma \xi \text{ 10,000 m}^2 \text{ ha}^{-1}$$

$$12\text{x}10^{-9} \text{ kg C } \mu\text{mol}^{-1} \text{ CO}_2 \quad \text{(A17)}$$

The g_c is calculated from g_s by first dividing by 1.6 to account for the difference in diffusivities between H_2O and CO_2 and using the perfect gas law to convert to units of moles; hence C_i is calculated:

$$C_i = C_a - A_n P/g_c \quad \text{(A18)}$$

where P is determined from elevation [Farquhar et al., 1980, 1989].

As both A_n and g_c are independently estimated, the isotopic discrimination against $^{13}CO_2$ during photosynthesis can be used as a check on the relative magnitudes of A_{max} and g_{max}. The $^{13}C/^{12}C$ ratio is commonly expressed as a $\delta^{13}C$ value calculated from

$$\delta^{13}C = {}^{13}R/{}^{13}R_0 - 1 \quad \text{(A19)}$$

[O'Leary, 1993]. Daily Δ is calculated for C_3 photosynthetic vegetation as

$$\Delta = 0.0044 + (0.027 - 0.0044)\, C_i/C_a \quad \text{(A20)}$$

and for C_4 photosynthetic vegetation as

$$\Delta = 0.0044 + (-0.0057 + 0.0087 - 0.0044)\, C_i/C_a \quad \text{(A21)}$$

assuming 29% of the CO_2 leaks from the bundle sheath cells of C_4 photosynthetic plants [O'Leary, 1993]. With the $\delta^{13}C$ of the air designated as an input parameter, the vegetation $\delta^{13}C$ is calculated according to Körner [1988] for C_3 photosynthesis:

$$\delta^{13}C = -0.0077 - \Delta\,(1 + -0.028) \quad \text{(A22)}$$

and for C_4 photosynthesis:

$$\delta^{13}C = -0.0077 - \Delta\,(1 + -0.014) \quad \text{(A23)}$$

where -0.028 and -0.014 are the mean $\delta^{13}C$ of C_3 species and C_4 species, respectively [Körner, 1988], and -0.0077 is the mean $\delta^{13}C$ of the air in 1987 [Keeling et al., 1989a]. The value of $^{13}R_a$ is taken to be 0.0112372 [Craig, 1957]. From $^{13}\delta$ of vegetation and PSN, the mass of ^{13}C is calculated and summed over the year. We assume there is no net isotopic fractionation of ^{13}C by autotrophic respiration; hence annual vegetation $\delta^{13}C$ is determined from PSN and the mass of ^{13}C.

Autotrophic and Heterotrophic Respiration

From LAI, initial values were calculated for various pools of carbon and nitrogen (Fig. 1). M_{lf} is

$$M_{lf} = \text{LAI} * 10{,}000 \text{ m}^2 \text{ ha}^{-1} / \text{SLA} \quad \text{(A24)}$$

where SLA is defined for each land cover type (Table 2). M_{fr} is set equal to M_{lf}, and M_{lit} is set to $5 \cdot M_{lf}$ to account for leaf, twig, coarse root, and fine root litter [Vogt et al., 1986]. Because sapwood is the only active tissue in the stems, M_{st} is related to LAI [Waring and Schlesinger, 1985], thus

$$M_{st} = \text{LAI } h\, \rho_{wood} / f_s \quad \text{(A25)}$$

where h is equal to $h_{max} \cdot (\text{LAI}/\text{LAI}_{max})$ (Table 2), f_s is assumed to be 0.35 $cm^2\ m^{-2}$ [Waring and Schlesinger, 1985], and ρ_{wood} is 250 kg C m^{-3}. For grasslands, M_{cr} is set equal to M_{lf} to obtain a 1:2 ratio of aboveground to belowground mass [D. S. Schimel, personal communication, 1994], whereas for forests, M_{cr} is equal to 0.33 M_{st}, and for shrubs, M_{cr} is set equal to 0.5 M_{st} using reasonable averages from biomass values reported in numerous studies [Cannell, 1982]. The nitrogen contents for leaves, stems and coarse roots, fine roots, litter, and soil are set equal to 0.02 M_{lf}, 0.005 M_{lf}, 0.01 M_{lf}, 0.02 M_{lit}, and 0.056 M_{soil}, respectively. The nitrogen cycle is calculated on the annual time step and controls allocation of carbon and nitrogen for future years (Figure 1), hence for a single-year simulation, BIOME-BGC is not regulated by the nitrogen pools, in contrast to some other ecosystem models. However, the important effects of leaf nitrogen on photosynthetic rates and stomatal conductances [Schulze et al., 1994; Kelliher et al., 1995] are approximated for each land cover type by differences in A_{max} and g_{max} (Table 2).

Maintenance respiration rates are calculated by

$$R_{st} = r_{st} \exp(\beta_m T_{air})\, M_{st} \quad \text{(A26)}$$

$$R_{cr} = r_{cr} \exp(\beta_m T_{soil})\, M_{cr} \quad \text{(A27)}$$

$$R_{fr} = r_{fr} \exp(\beta_m T_{soil})\, M_{fr} \quad \text{(A28)}$$

where r_{st}, r_{cr}, and r_{fr} were obtained from field data (median from numerous studies). The exponential temperature response of organisms is described in terms of a Q_{10}, which is the relative increase in rate for a 10°C increase in temperature. Maintenance respiration usually has a Q_{10} of about 2.0, so β_m was set at 0.069. R_{lf} (if active) is calculated using Tnight:

$$R_{lf} = r_{lf} \exp(\beta_m T_{night})\, [(\varsigma_{24} - \varsigma)/\varsigma_{24}]\, M_{lf} \quad \text{(A29)}$$

Total maintenance respiration (R, kg C $ha^{-1}\ d^{-1}$) is the sum of the daily amounts for leaves (nighttime only), stems, coarse roots, and fine roots.

If daily PSN is greater than total maintenance respiration, then the difference is allocated among leaves, stems, coarse roots and fine roots using constant allocation parameters [Running and Coughlan, 1988]. The amount of respiration used for growth is

$$G_{lf} = g_{lf}\, \eta_{lf}\, (\text{PSN} - R) \quad \text{(A30)}$$

$$G_{st} = g_{st}\, \eta_{st}\, (\text{PSN} - R) \quad \text{(A31)}$$

$$G_{cr} = g_{cr}\, \eta_{cr}\, (\text{PSN} - R) \quad \text{(A32)}$$

$$G_{fr} = g_{fr}\, \eta_{fr}\, (\text{PSN} - R) \quad \text{(A33)}$$

Since there is little information about allocation patterns and growth respiration rates, for this study, g_{lf}, g_{st}, g_r, and g are assumed to be 0.33 [Sprugel et al., 1995]. Thus differences in allocation among plant organs do not affect total daily growth respiration; total autotrophic respiration is the sum of total maintenance and growth respiration.

R_h is the sum of R_{soil} and R_{lit},, both of which are limited by soil

temperature and soil moisture content [Parton et al., 1987]. A soil temperature multiplier $f(T_{soil})$ is calculated by

$$f(T_{soil}) = \exp [\beta_s (T_{soil} - 26.0^\circ)] \quad \text{(A34)}$$

where β_s is set to achieve a Q_{10} of 2.4 [Raich and Schlesinger, 1993] and 26.0°C is the reference soil temperature from Taylor et al. [1989]. The $f(\Theta)$ is set equal to unity if the ratio $\Theta/\Theta_{max} > 0.75$, and is set to 0.1 when $\Theta/\Theta_{max} < 0.25$, and a linear interpolation between the above points is used for $0.75 > \Theta/\Theta_{max} > 0.25$. R_{soil} is

$$R_{soil} = r_{soil}\, f(T_{soil})\, f(\Theta)\, M_{soil} \quad \text{(A35)}$$

where r_{soil} is set equal to 0.00035 kg C kg^{-1} C d^{-1} (a combination of the active and slow soil carbon pools in the Century model [Parton et al., 1987]). The nitrogen concentration of the litter is assumed to be one half of the leaf nitrogen concentration. Litter lignin and nitrogen concentrations are used to calculate a lignin:N ratio (L, kg lignin per kg N). The r_{lit} is calculated by

$$r_{lit} = 1 - \exp\{(3/365) \ln[(0.999\, L + 45.7)/100]\} \quad \text{(A36)}$$

where 3/365 converts the above equation from Taylor et al. [1989] to a daily time step. Then

$$R_{lit} = r_{lit}\, f(T_{soil})\, f(\Theta)\, M_{lit} \quad \text{(A37)}$$

M_{lit} and M_{soil} are decreased by the amount of respiration daily. NPP is equal to PSN - R_a, and NEE is equal to PSN - R_a - R_h, by definition.

Annual Time Step

The annual time step of BIOME-BGC (Figure 1) is similar to that of FOREST-BGC [Running and Gower, 1991], with modifications as described below. All of the processes of the annual time step of BIOME-BGC are called on day 365 of the year (Figure 1). Via the decomposition of leaf and fine root litter, the litter C:N ratio gradually decreases. If the C:N ratio is greater than a critical value (25 from Parton et al. [1987]), then nitrogen is immobilized, and the transfer of litter nitrogen and carbon to the soil requires nitrogen from the available N pool. If the C:N ratio is less than the critical value, then nitrogen is mineralized and transferred to the available nitrogen pool. Then 30% of the original litter carbon (from the lignocellulose hypothesis of Melillo et al. [1989]) and an amount of litter nitrogen that maintains the critical C:N ratio is transferred to the soil carbon and nitrogen pools, respectively. Soil carbon turnover releases soil nitrogen into the available nitrogen pool with a C:N ratio of 12 [Parton et al., 1987]. If the amount of available nitrogen is high, then some nitrogen is lost from the system [Johnson, 1992]. Each year, nitrogen is added to the available nitrogen pool through N_2 fixation, N deposition, and retranslocation of nitrogen from senescing leaves (assumed to be 50% of leaf nitrogen). The net nitrogen available is then allocated to the various vegetation pools.

From the ratio of NPP and the sum of N inputs and N retranslocation minus N losses, carbon and nitrogen are allocated to leaves, stems, coarse roots, and fine roots [Running and Gower, 1991]. Transfer of available carbon to storage carbon (Figure 1) is not implemented in this global version of BIOME-BGC but is important for time series analyses [Hunt et al. 1991b]. The use of an annual time step called on day 365 of the year was originally designed for northern latitudes where vegetation activity is minimal during the winter months. In subsequent model simulations, we will replace annual allocation with a more realistic specification for both hemispheres depending on land cover type.

Appendix B: Biomass Burning as a Source of CO_2

In this study, we have included one additional CO_2 source for the TM2. Emissions from biomass burning produce significant seasonal variation of atmospheric CO_2 in the tropics and the southern hemisphere as shown, for example, by Iacobellis et al. [1994]. We have constructed a time-dependent biomass burning source from the global data set of Hao and Liu [1994]. These authors estimated the spatial and temporal variation of biomass burning on the basis of Food and Agriculture Organization survey data, global vegetation and cultivation maps [Matthews, 1983], and on published data of biomass density. Emissions from deforestation, savanna burning, and shifting cultivation were distributed monthly on the basis of surface ozone concentrations during a 6-month dry season, which in turn was determined on the basis of rainfall data from Jaeger [1976]. The burning of fuelwood and agricultural residues were assumed to be constant over the year. Hao and Liu [1994] did not provide the spatial distribution for Australian emissions; therefore, we derived this from information provided to us by W. M. Hao (personal communication, 1993).

Hao and Liu [1994] provide biomass burning totals appropriate for the late 1970s. On the basis of further information provided in their study, we increased the deforestation totals by 36, 22, and 88% in tropical America, tropical Africa and tropical Asia, respectively, and increased fuel wood burning uniformly by 34% to provide totals applicable to the late 1980s for our study. The total increase was only 0.19 Pg C per year, about half of it in the nonseasonal fuelwood burning. We used a factor of 0.45 g C per g dry biomass [Hao et al., 1990] to convert from biomass to carbon in CO_2. In our final source, global CO_2 emissions totaled 2.62 Pg C per year, with savanna fires accounting for almost half of the total. Changes in NPP associated with loss and recovery of plants owing to biomass burning are roughly accounted for in our NDVI model by the biweekly satellite NDVI data, and approximately in the BIOME-BGC model, which used the annual maximum NDVI to establish the maximum LAI, and hence biomass, in each grid cell. On the other hand, to maintain a steady state in each cell, our R_h fluxes should be reduced by the amount of CO_2 lost to biomass burning. However, biomass burning is much more seasonal than the R_h fluxes, according to Hao and Liu [1994], most burning occurs in the 3 months of the dry season and involves only 6.9×10^{12} m^2, or about 13% of the area of tropical vegetation. Thus, as we are concerned only with the seasonality in our simulations, we have simply added the biomass burning fluxes, neglecting a small adjustment to the R_h source. We remapped the 5° x 5° source to our 7.83° x 10° transport model grid for the TM2 model simulations.

Acknowledgments. Funding for this research was provided by NASA grant NAGW-2987 to C. D. Keeling and S. C. Piper, Electric Power Research Institute grant RP8011-20 to C. D. Keeling, DOE NIGEC grant W/GEC 91-022 to C. D. Keeling, NASA Earth Observing System Contract NAS5-31368 to S. W. Running, NASA grant NAGW-3151 to R. R.

Nemani, and NASA grant NAG 5-2065 to E. R. Hunt Jr. Computations at Scripps were additionally supported by San Diego Supercomputer Center and the S. 1. O. block grant administered by Steven Constable. We thank Elisabeth Stewart from the Scripps Institution of Oceanography and Hal Dorsman, Matt Rollins, Peter Thornton, Joe White, and Kim Hodgson from the University of Montana. We also thank Martin Heimann from the Max Planck Institute for Meteorology for providing us with the atmospheric transport model, TM2; David Miskus and colleagues at the U. S. Climate Prediction Center and Mike Changery at the U. S. National Climatic Data Center for help in interpreting the daily climate data and quality flags, Rachel Pinker of the University of Maryland for supplying the satellite-derived PAR data, Ye Qi from the Theory Center of Cornell University for his work on the Gallo-NDVI data; and Cort Willmott of the University of Delaware for supplying us with his climate data gridding routine.

References

Andres, R. J., G. Marland, T. Boden, and S. Bischof, Carbon dioxide emissions from fossil fuel consumption and cement manufacture, and an estimate of their isotopic composition and latitudinal distribution, in *Proceedings of the 1993 Global Change Institute on the Carbon Cycle*, edited by T. Wigley and D. Schimel, pp. 1751-1991, Cambridge Univ. Press, New York, 1995.

Asrar, G., R. B. Myneni, and B. J. Choudhury, Spatial heterogeneity in vegetation canopies and remote sensing of absorbed photosynthetically active radiation, *Remate Sens. Environ.*, *41*, 85-101, 1992.

Baldocchi, D. D., and T. P. Meyers, Trace gas exchange above the floor of a deciduous forest, 1, Evaporation and CO_2 efflux, *J. Geophys. Res.*, *96*, 7271-7285, 1991.

Bonan, G. B., Land-atmosphere CO_2 exchange simulated by a land surface process model coupled to an atmospheric general circulation model, *J. Geophys. Res.*, *100*, 2817-2831, 1995.

Cannell, M. G. R., *World Forest Biomass and Primary Production Data*, 391 pp., Academic Press, San Diego, Calif., 1982.

Ciais, P., P. P. Tans, J. W. C. White, M. Trolier, R. J. Francey, J. A. Berry, D. R. Randall, P. J. Sellers, J. G. Collatz, and D. S. Schimel, Partitioning of ocean and land uptake of CO_2 as inferred by $\delta^{13}C$ measurements from the NOAA Climate Monitoring and Diagnostics Laboratory global air sampling network, *J. Geophys. Res.*, *100*, 5051-5070, 1995.

Conway, T. J., P. P. Tans, L. S. Waterman, and K. W. Thoning, Evidence for interannual variability of the carbon cycle from the National Oceanic and Atmospheric Administration Climate Monitoring and Diagnostics Laboratory of Global Air Sampling Network, *J. Geophys. Res.*, *99*, 22821-22855, 1994.

Coughlan, J. C., and S. W. Running, Regional ecosystem simulation: A general model for simulating snow accumulation and melt in mountainous terrain, *Landscape Ecol.*, in press, 1996.

Craig, H., Isotopic standards for carbon and oxygen and correction factors for mass-spectrographic analysis of carbon dioxide, *Geochim. Cosmachim. Acta*, *12*, 133-149, 1957.

Cuming, M. J., and B. A. Hawkins, TERDAT: The FNOC system for terrain data extraction and processing, *Tech. Rep. MII Project M-254*, 2nd ed., Fleet Numer. Oceanogr. Cent., Monterey, Calif., 1981.

DeFries, R. S., and J. R. G. Townsend, NDVI-derived land cover classifications at a global scale, *Int. J. Remote Sens.*, *15*, 3567-3586, 1994.

Denning, A. S., I. Y. Fung, and D. Randall, Latitudinal gradient of atmospheric CO_2 due to seasonal exchange with land biota, *Nature*, *376*, 240-243, 1995.

Ehleringer, J. R., and O. Björkman, Quantum yields for CO_2 uptake in C_3 and C_4 plants: Dependence on temperature, CO_2 and O_2 concentrations, *Plant Physiol.*, *59*, 86-90, 1977.

Farquhar, G. D., S. von Caemmerer, and J. A. Berry, A biochemical model of photosynthetic CO_2 assimilation in leaves of C_3 plants, *Planta*, *149*, 78-90, 1980.

Farquhar, G. D., J. R. Ehleringer, and K. T. Hubick, Carbon isotope discrimination and photosynthesis, *Annu. Rev. Plant Physiol. Plant Mol. Biol.*, *40*, 503-537, 1989.

Francey, R. J., P. P. Tans, C. E. Allison, I. G. Enting, J. W. C. White, and M. Trolier, Changes in oceanic and terrestrial carbon uptake since 1982, *Nature*, *373*, 326-330, 1995.

Fung, I. Y., C. J. Tucker, and K. C. Prentice, Application of advanced very high resolution radiometer vegetation index to study atmosphere-biosphere exchange of CO_2, *J. Geophys. Res.*, *92*, 2999-3015, 1987.

Gallo, K. P., *Experimental Calibrated Global Vegetation Index from NOAA AVHRR, 1985-1991*, NOAA/Nat. Geophys. Data Cent., Boulder, Colo., 1992.

Gates, D. M., *Biophysical Ecology*, 611 pp., Springer-Verlag, New York, 1980.

Glassy, J. M., and S. W. Running, Validating diurnal climatology logic of the MT-CLIM model across a climatic gradient in Oregon, *Ecol. Appl.*, *4*, 248-257, 1994.

Goward, S. M., C. J. Tucker, and D. G. Dye, North American vegetation patterns observed with the NOAA-7 advanced very high resolution radiometer, *Vegetatio*, *64*, 3-14, 1985.

Hao, W. M., and M. -H. Liu, Spatial and temporal distribution of tropical biomass burning, *Global Biogeochem. Cycles*, *8*, 495-503, 1994.

Hao, W. M., M. -H. Liu, and P. J. Crutzen, Estimates of annual and regional releases of CO_2 and other trace gases to the atmosphere from fires in the tropics, based on FAO statistics for the period 1975-1980, in *Fire in the Tropical Biota*, *Ecol. Stud.*, vol. 84, edited by J. G. Goldhammer, pp. 440-462, Springer-Verlag, New York, 1990.

Heimann, M., The global atmospheric tracer model TM2,*Tech. Rep. 10*, 53 pp., *Dsch. Klimarechenzentrum*, Hamburg, Germany, 1995.

Heimann, M., and C. D. Keeling, A three-dimensional model of atmospheric CO_2 transport based on observed winds, 2, Model description and simulated tracer experiments, in *Aspects of Climate Variability in the Pacific and the Western Americas*, *Geophys. Monogr. Ser.*, vol. 55, edited by D. H. Peterson, pp. 237-275, AGU, Washington, D. C., 1989.

Heimann, M., C. D. Keeling, and C. J. Tucker, A three-dimensional model of atmospheric CO_2 transport based on observed winds, 3, Seasonal cycle and synoptic time scale variations, in Aspects of Climate Variability in the Pacific and the Western Americas, *Geophys. Monogr.*, vol. 55, edited by D. H. Peterson, pp. 277-303, AGU, Washington, D. C., 1989.

Houghton, R. A., The worldwide extent of land-use change, *Bioscience*, *44*, 305-313, 1994.

Hunt, E. R., Jr., and S. W. Running, Simulated dry matter yields for aspen and spruce stands in the North American boreal forest, *Can. J. Remote Sens.*, *18*, 126-133, 1992a.

Hunt, E. R., Jr. and S. W. Running, Effects of climate and lifeform on dry matter yield (ϵ) from simulations using BIOME-BGC, paper presented at *IGARSS '92, International Geoscience and Remote Sensing Symposium*, Houston, Texas, 1992b.

Hunt, E. R., Jr., C. A. Fedderer, and S. W. Running, Extrapolating plant water flow resistances and capacitances to regional scales, *Agric. For. Meterol.*, *54*, 169-195, 1991a.

Hunt, E. R., Jr., F. E. Martin, and S. W. Running, Simulating the effects of climatic variation on stem carbon accumulation of a ponderosa pine stand: comparison with annual growth increment data, *Tree Physiol.*, *9*, 161-171, 1991b.

Iacobellis, S. F., R. Frouin, H. Razafimpanilo, R. C. J. Somerville, and S. C. Piper, North African savanna fires and atmospheric carbon dioxide, *J. Geophys. Res.*, *99*, 8321-8334, 1994.

Jaeger, L., Monatskarten des Niederschlags für die ganze Erde, *Ber. 139*, Bd. 18, *Dtsch. Wetterdienstes*, Offenbach, Main, Germany, 1976.

Jarvis, P. G., and J. W. Leverenz, Productivity of temperate, deciduous and evergreen forests, in *Encyclopedia of Plant Physiology, New Ser.*, vol. 12D, edited by O. L. Lange et al., pp. 233-280, Springer-Verlag, New York, 1984.

Johnson, D. W., Nitrogen retention in forest soils, *J. Environ. Qual.*, *21*, 1-12, 1992.

Keeling, C. D., R. B. Bacastow, A. F. Carter, S. C. Piper, T. P. Whorf, M. Heimann, W. G. Mook, and H. Roeloffzen, A three-dimensional model of atmospheric CO_2 transport based on observed winds, 1, Analysis of observational data, in *Aspects of Climate Variability in the Pacific and the Western Americas*, *Geophys. Monogr. Ser.*, vol. 55,

edited by D. H. Peterson, pp. 165-236, AGU, Washington, D. C., 1989a.

Keeling, C. D., S. C. Piper, and M. Heimann, A three-dimensional model of atmospheric CO_2 transport based on observed winds, 4, Mean annual gradients and interannual variations, in *Aspects of Climate Variability in the Pacific and the Western Americas*, *Geophys. Monogr. Ser.*, vol. 55, edited by D. H. Peterson, pp. 305-363, AGU, Washington, D. C., 1989b.

Keeling, C. D., T. P. Whorf, M. Wahlen, J. van der Plicht, Interannual extremes in the rate of rise of atmospheric carbon dioxide since 1980, *Nature*, *375*, 666-670, 1995.

Kelliher, F. M., R. Leuning, M. R. Raupach, and E. -D. Schulze, Maximum conductances for evaporation from global vegetation types, *Agric. For. Meterol.*, *73*, 1-16, 1995.

Kineman, J. J., and M. A. Ohrenschall, Global Ecosystems Database, version 1.0, A documentation manual [CD-ROM], *Key Geophys. Rec. Doc. 27*, Nat. Geophys. Data Cent., Boulder, Colo., 1992.

Körner, C., G. D. Farquhar, and Z. Roksandic, A global survey of carbon isotope discrimination in plants from high altitude, *Oecologia*, *74*, 623-632, 1988.

Korol, R. L., S. W. Running, K. S. Milner, and E. R. Hunt Jr., Testing a mechanistic carbon balance model against observed tree growth, *Can. J. For. Res.*, *21*, 1098-1105, 1991.

Kumar, M., and J. L. Monteith, Remote sensing of crop growth, in *Plants and the Daylight Spectrum*, edited by H. Smith, pp. 133-144, Academic, San Diego, Calif., 1981.

Leemans, R., Possible changes in natural vegetation patterns due to a global warming, *IIASA Working Pap. WP-90-08 and Publ.108*, Int. Inst. of Appl. Syst. Anal., Laxenburg, Austria, 1990.

Leemans, R., and W.P. Cramer, The IIASA database for mean monthly values of temperature, precipitation, and cloudiness on a global terrestrial grid, *Rep. RR-91-18*, 62 pp., Int. Inst. for Appl. Syst. Anal., Laxenburg, Austria, 1991.

Legates, D.R., A climatology of global precipitation, *Publ. Climatology*, *40*, 1-85, 1987.

Loveland, T. R., J. W. Merchant, D. Ohlen, and J. F. Brown, Development of a land-cover characteristics database for the conterminous U.S., *Photogramm. Eng. Remote Sens.*, *57*, 1453-1463, 1991.

Lüdeke, M. K., et al., The Frankfurt biosphere model: A global process-oriented model of seasonal and long-term CO_2 exchange between terrestrial ecosystems and the atmosphere, I, Model description and illustrative results for cold deciduous and boreal forest, *Clim. Res.*, *4*, 143-166, 1994.

Matthews, E., Global vegetation and land use: New high-resolution data bases for climate studies, *J. Clim. Appl. Meteorol.*, *22*, 474-487, 1983.

McMurtrie, R. E., R. Leuning, W. A. Thompson, and A. M. Wheeler, A model of canopy photosynthesis and water use incorporating a mechanistic formulation of leaf CO_2 exchange, *For. Ecol. Manage.*, *52*, 261-278, 1992.

Melillo, J. M., J. D. Aber, A. E. Linkins, A. Ricca, B. Fry, and K. J. Nadelhoffer, Carbon and nitrogen dynamics along the decay continuum: Plant litter to soil organic matter, in *Ecology of Arable Land*, edited by M. Clarholm and L. Bergström, pp. 53-62, Kluwer Acad., Norwell, Mass., 1989.

Melillo, J. M., A. D. McGuire, D. W. Kicklighter, B. Moore III, C. J. Vorosmarty, and A. L. Schloss, Global climate change and terrestrial net primary production, *Nature*, *363*, 234-240, 1993.

National Geophysical Data Center (NGDC), ETOPO5: Digital relief of the surface of the Earth, map, Nat. Geophys. Data Cent., Boulder, Colo, 1988.

Nemani, R. R., and S. W. Running, Testing a theoretical climate-soil-leaf area hydrologic equilibrium of forests using satellite data and ecosystem simulation. *Agric. For. Meteorol.*, *44*, 245-260, 1989a.

Nemani, R. R., and S. W. Running, Estimation of regional surface resistance to evapotranspiration from NDVI and Thermal-IR AVHRR data, *J. Appl. Meteorol.*, *28*, 276-284, 1989b.

Nemani, R. R., and S. W. Running, Satellite monitoring of global land cover changes and their impact on climate. *Clim. Change*, *31*, 395-413, 1995.

Nemani, R. R., and S. W. Running, Global vegetation cover changes from coarse resolution satellite data. *J. Geophys. Res.*, *101*, 7145-7162, 1996.

Nepstad, D. C., C. R. de Carvalho, E. A. Davidson, P. H. Jipp, P. A. Lefebvre, C. H. Negreiros, E. D. da Silva, T. A. Stone, S. E. Trumbore, and S. Vieira, The role of deep roots in the hydrological and carbon cycles of Amazonian forests and pastures, *Nature*, *372*, 666-669, 1994.

O'Leary, M. H., Biochemical basis of carbon isotope fractionation, in *Stable Isotopes and Plant Carbon-Water Relations*, edited by J. R. Ehleringer et al., pp. 19-28, Academic, San Diego, Calif., 1993.

Parton, W. J., D. S. Schimel, C. V. Cole, and D. S. Ojima, Analysis of factors controlling soil organic matter levels in Great Plains grasslands, *Soil Sci. Soc. Am. J.* , *51*, 1173-1179, 1987.

Parton, W. J., et al., Observations and modeling of biomass and soil organic matter dynamics for the grassland biome worldwide, *Global Biogeochem. Cycles*, *7*, 785-809, 1993.

Pierce, L. L., J. Walker, T. I. Dowling, T. R. McVicar, T. J. Hatton, S. W. Running, and J. C. Coughlan, Ecohydrological changes in the Murray-Darling basin, III, A simulation of regional hydrological changes, *J. Appl. Ecol.*, *30*, 283-294, 1993.

Pinker, R. T., and I. Laszlo, Modeling surface solar irradiance for satellite applications on a global scale, *J. Appl. Meteorol.*, *31*, 194-211, 1992.

Pinker, R. T., I. Laszlo, C. H. Whitlock, and T. P. Charlock, Radiative flux opens new window on climate research, *Eos Trans. AGU*, *76*, 145, 155, and 158, 1995.

Piper, S. C., Construction and description of a gridded global data set of daily temperature and precipitation for terrestrial biospheric modeling, *S.I.O. Ref. Ser. 94-13*, 67 pp., Scripps Inst. of Oceanogr., Univ. of Calif., San Diego, 1995.

Piper, S. C., and E. F. Stewart, A gridded global data set of daily temperature and precipitation for terrestrial biospheric modelling, *Global Biogeochem. Cycles*, in press, 1996.

Post, W. M., W. R. Emanuel, P. J. Zinke, and A. G. Stangenberger, Soil carbon pools and world life zones, *Nature*, *298*, 156-159, 1982.

Potter, C. S., J. T. Randerson, C. B. Field, P. A. Matson, P. M. Vitousek, H. A. Mooney, and S. A. Klooster, Terrestrial ecosystem production: A process model based on global satellite and surface data, *Global Biogeochem. Cycles*, *7*, 811-841, 1993.

Raich, J. W., and C. S. Potter, Global patterns of carbon dioxide emissions from soils, *Global Biogeochem. Cycles*, *9*, 23-36, 1995.

Raich, J. W., and W. H. Schlesinger, The global carbon dioxide flux in soil respiration and its relationship to vegetation and climate, *Tellus Ser. B*, *44*, 81-99, 1993.

Rastetter, E. B., M. G. Ryan, G. R. Shaver, J. M. Melillo, K. J. Nadelhoffer, J. E. Hobbie, and J. D. Aber, A general biogeochemical model describing the responses of the C and N cycles in terrestrial ecosystems to changes in CO_2, climate, and N deposition, *Tree Physiol.*, *9*, 101-126, 1991.

Rastetter, E. B., A. W. King, B. J. Cosby, G. M. Hornberger, R. V. O'Neill, and J. E. Hobbie, Aggregating fine-scale ecological knowledge to model coarser-scale attributes of ecosystems, *Ecol. Appl.*, *2*, 55-70, 1992.

Rollins, M. G., Comparing measured and simulated H_2O and CO_2 fluxes spatially for the 15 km by 15 km FIFE site, M.S. thesis, 66 pp., Univ. of Mont., Missoula, 1995.

Ropelewski, C. F., and M. S. Halpert, Global and regional scale precipitation patterns associated with the El Niño/Southern Oscillation, *Mon. Weather Rev.*, *115*, 1606-1626, 1987.

Running, S. W., Testing FOREST-BGC ecosystem process simulations across a climatic gradient in Oregon, *Ecol. Appl.*, *4*, 238-247, 1994.

Running, S. W., and J. C. Coughlan, A general model of forest ecosystem processes for regional application, *Ecol. Modell.*, *42*, 125-154, 1988.

Running, S. W., and S. T. Gower. FOREST-BGC, A general model of forest ecosystem processes for regional applications, II, Dynamic carbon allocation and nitrogen budgets, *Tree Physiol.*, *9*, 147-160, 1991.

Running, S. W., and E. R. Hunt Jr., Generalization of a forest ecosystem process model for other biomes, BIOME-BGC, and an application for

global-scale models, in *Scaling Physiological Processes: Leaf to Globe*, edited by J. R. Ehleringer and C. Field, pp. 141-158, Academic, San Diego, Calif., 1993.

Running, S. W., and R. R. Nemani, Relating seasonal patterns of the AVHRR vegetation index to simulated photosynthesis and transpiration of forests in different climates, *Remote Sens. Environ.*, *24*, 347-367, 1988.

Running, S. W., R. R. Nemani, and R. D. Hungerford, Extrapolation of synoptic meteorological data in mountainous terrain and its use for simulating forest evapotranspiration and photosynthesis *Can. J. For. Res.*, *17*, 472-483, 1987.

Running, S. W., T. R. Loveland, L. L. Pierce, R. R. Nemani, and E. R. Hunt Jr., A remote sensing based vegetation classification logic for global land cover analysis. *Remote Sens. Environ.*, *51*, 39-48, 1995.

Saxton, K. E., W. J. Rawls, J. S. Romberger, and R. I. Papendick, Estimating generalized soil-water characteristics from texture, *Soil Sci. Soc. Am. J.*, *50*, 1031-1036, 1986.

Schimel, D. S., Terrestrial ecosystems and the carbon cycle, *Global Change Biol.*, *1*, 77-91, 1995.

Schimel, D. S., B. H. Braswell, E. A. Holland, R. McKeown, D. S. Ojima, T. H. Painter, W. J. Parton, and A. R. Townsend, Climatic, edaphic, and biotic controls over storage and turnover of carbon in soils, *Global Biogeochem. Cycles*, *8*, 279-293, 1994.

Schulze E. -D., F. M. Kelliher, C. Körner, J. Lloyd, and R. Luening, Relationships among maximum stomatal conductance, ecosystem surface conductance, carbon assimilation rate, and plant nutrition, *Annu. Rev. Ecol. Syst.*, *25*, 629-660, 1994.

Sellers, P. J., J. A. Berry, G. J. Collatz, C. B. Field, and F. G. Hall, Canopy reflectance, photosynthesis, and transpiration, III, A reanalysis using improved leaf models and a new canopy integration scheme, *Remote Sens. Environ.*, *42*, 187-216, 1992.

Sellers, P. J., C. J. Tucker, G. J. Collatz, S. O. Los, C. O. Justice, D. A. Dazlich, and D. A. Randall, A global 1° by 1° data set for climate studies, 2, The generation of global fields of terrestrial biophysical parameters from the NDVI, *Int. J. Remote Sens.*, *15*, 3519-3545, 1994.

Sellers, P. J., S. O. Los, C. J. Tucker, C. O. Justice, D. A. Dazlich, C. Zhang, G. J. Collatz, and D. A. Randall, A revised land surface parameterization (SiB2) for atmospheric GCMs, II, The generation of global fields of terrestrial biophysical parameters from satellite data, *J. Climate*, *9*, 706-737, 1996.

Shepard, D., A two-dimensional interpolation function for irregularly-spaced data, *Proceedings of the Twenty-Third ACM National Conference*, pp. 517-524, Brandon Syst., Princeton, N.J., 1968.

Spanner, M. A., L. L. Pierce, S. W. Running, and D. L. Peterson, The seasonality of AVHRR data of temperate coniferous forests: Relationship with leaf area index, *Remote Sens. Environ.*, *33*, 97-112, 1990.

Sprugel, D. G., M. G. Ryan, J. Renée Brooks, K. A. Vogt, and T. A. Martin, Respiration from the organ level to the stand level, in *Resource Physiology of Conifers*, edited by W. K. Smith and T. M. Hinkley, pp. 255-299, Academic, San Diego, Calif., 1995.

Sundquist, E. T., The global carbon dioxide budget, *Science*, *259*, 934-941, 1993.

Taylor, B. R., D. Parkinson, and W. F. J. Parsons, Nitrogen and lignin content as predictors of litter decay rates: A microcosm test, *Ecology*, *70*, 97-104, 1989.

Teeri, J. A., The climatology of the C_4 photosynthetic pathway, in *Topics in Plant Biology*, edited by O. T. Solbrig et al., pp. 356-374, Columbia Univ. Press, New York, 1977.

Vogel, J. C., Variability of carbon isotope fractionation during photosynthesis, in *Stable Isotopes and Plant Carbon-Water Relations*, edited by J. R. Ehleringer et al., pp. 29-46, Academic, San Diego, Calif., 1993.

Vogt, K. A., C. C. Grier, and D. J. Vogt, Production, turnover, and nutrient dynamics of above- and belowground detritus of world forests, *Adv. Ecol. Res.*, *15*, 303-377, 1986.

Warnant, P., L. François, D. Strivay, and J.-C. Gérard, CARAIB: A global model of terrestrial biological productivity, *Global Biogeochem. Cycles*, *8*, 255-270, 1994.

Waring, R. H., and W. H. Schlesinger, *Forest Ecosystems, Ecology and Management*, 340 pp., Academic, San Diego, Calif., 1985.

Webb, R. S., C. E. Rosenzweig, and E. R. Levine, Specifying land surface characteristics in general circulation models: soil profile data set and derived water-holding capacities, *Global Biogeochem. Cycles*, *7*, 97-108, 1993.

Willmott, C. J., C. M. Rowe, and W. D. Philpot, Small-scale climate maps: a sensitivity analysis of some common assumptions associated with grid-point interpolation and contouring, *Am. Geogr.*, *12*, 5-16, 1985.

World Climate Data Programme, *Climate System Monitoring, Monthly Bulletin*, 1987-1 to 12, Geneva, Switzerland, 1987.

World Climate Data Programme, *Climate System Monitoring, Monthly Bulletin*, 1988-1 to 4, Geneva, Switzerland, 1988.

Zheng, D., E. R. Hunt Jr., and S. W. Running, A daily soil temperature model derived from air temperature and precipitation for continental applications, *Climate Res.*, *2*, 183-191, 1993.

Zobler, L., A world soil file for global climate modeling, *Tech. Memo. 87802*, Nat. Aeronaut. and Space Admin., Greenbelt, Md., 1986.

E. Raymond Hunt Jr., Department of Botany, University of Wyoming, P.O Box 3165, Laramie, WY 32071-3165. (e-mail: erhunt@uwyo.edu)

C. D. Keeling and S. C. Piper, Scripps Institution of Oceanography, La Jolla, CA 92093-0220. (e-mail: cdkeeling@ucsd.edu; piper@cdrgsun.ucsd.edu)

R. Nemani and S. W. Running, School of Forestry, University of Montana, Missoula, MT 59812-1063. (e-mail: nemani@ntsg.umt.edu; swr@ntsg.umt.edu)

R. D. Otto, Institut für Physikalische und Theoretische Chemie, J. W. Goethe-Universität Frankfurt am Main, Marie-Curie-Str. 11, D-60439 Frankfurt am Main, Germany.

(Received January 30, 1996; revised May 29, 1996; accepted May 30, 1996.)